Numerical and experimental investigations on mooring loads of a marine fish farm in waves and current

Yugao Shen[a,b,*], Marilena Greco[a,b,c], Odd M. Faltinsen[a,b], Ivar Nygaard[d]

[a] *Department of Marine Technology, Norwegian University of Science and Technology (NTNU), Trondheim, NO-7491, Norway*
[b] *Centre for Autonomous Marine Operations and Systems (AMOS), NTNU, Trondheim, NO-7491, Norway*
[c] *CNR-INSEAN, Marine Technology Research Institute, Rome, Italy*
[d] *Sintef Ocean, Trondheim, Norway*

Abstract

A realistic aquaculture fish farm system in both regular and irregular waves is investigated by numerical simulations and model tests. The main purpose is to develop a reliable numerical tool and in this respect to investigate the survival conditions of the system. The structural and hydrodynamic modelings of the system are briefly introduced. Numerical sensitivity analysis is performed to investigate which physical parameters are dominant when modeling the system.

The considered fish farm comprises a floating collar with two concentric tubes, a flexible net cage including a cylindrical part and a conical part with a center point weight at the bottom, and a sinker tube attached directly to the net. The system is moored with a complex mooring system with bridle lines, frame lines and anchor lines, supported by buoys.

The mooring loads in the front two anchor lines and bridle lines are investigated in detail. Numerical results are first validated by the experimental data. Both numerical and experimental results show that one of the bridle lines experiences larger load than the rest of the mooring lines, which is surprising. Then a sensitivity analysis is carried out. The mooring loads are not sensitive to the majority of the parameters. The flow reduction factor in the rear part of the net is the most important parameter for the anchor loads. Modeling the floating collar as a rigid body has a small effect on the anchor loads but not for the bridle lines as it will alter the force distribution between bridles. The mooring loads are not sensitive to the wave load model for the floating collar in both regular and irregular seas and modeling the floating collar as elastic with zero frequency hydrodynamic coefficients is enough to give reliable results.

Finally, the survival conditions of the fish farms with different set-ups is studied. Numerical results indicate that the dominant limitation to move the conventional fish farms to more exposed sea regions is the large volume reduction of the net cage. The existing mooring system can be applied in offshore regions as long as the bridle lines are properly designed. The maximum stress in the floating collar is moderate compared with the yield stress.

Keywords: Realistic aquaculture fish farm, current, regular waves, irregular waves, survival conditions

1. Introduction

Due to limited nearshore area and great impact to local ecosystem, the aquaculture industry is trying to move the fish farms from nearshore to more exposed sea regions where waves and current are stronger. This will greatly increase the probability of structural failure. Although new fish farm concepts were proposed to operate in exposed areas, it is still valuable to check the operational limits of the existing fish farm concepts and possibilities to use them in exposed regions. Among many existing concepts, we will focus on the floating collar fish farm, which is the most commonly used concept nowadays. Each unit in a fish farm typically comprises a floating collar with two concentric tubes, a flexible net cage, a sinker tube and possible chains connecting the sinker tube and the floating collar. The system is moored with a complex mooring system with bridle lines, frame lines and anchor lines, supported by spar type buoys. In reality, there may exist multiple cages at sites with cages arranged in single

*Corresponding author
Email address: yugao.shen@ntnu.no (Yugao Shen)

or double rows. This will have an influence, for instance, on the steady inflow (current) due to the shadowing effects from the upstream cages, compared with a single cage system.

Many investigations have been done to examine the responses of a floating fish farm by model tests and numerical simulations. The system is often simplified to reduce the complexity. For example Lader and Fredheim (2006) applied a truss model to investigate the responses of a two-dimensional flexible net sheet exposed to waves and current. Zhao et al. (2008) presented an experimental and numerical study of hydrodynamic characteristics of submerged flexible plane nets in waves. Moe et al. (2010) applied the commercial software ABAQUS to estimate the drag force on a circular-flexible-bottomless net cage in current. Similar net cage set-up in waves and current were studied experimentally and numerically by Huang et al. (2006), Zhao et al. (2007) and Lee et al. (2008). The hydrodynamic behaviors of multiple net cages in waves and current were investigated numerically by Xu et al. (2012, 2013b). Zhao et al. (2015) also performed an experimental study on flow velocity and mooring loads for multiple net cages in steady current. The dynamic responses of a net cage in irregular waves were analyzed by Dong et al. (2010) and Xu et al. (2011). Studies of the hydrodynamic behavior of a submersible net cage in waves and current were also performed by Xu et al. (2013a).

Common to previous works is that the hydrodynamic part of the problem is often over-simplified, for instance the floater was assumed to be rigid and the hydrodynamic forces of the floater were predicted by two-dimensional (2D) hydrodynamic strip theory. The viscous force on the net cage was predicted by Morison's equation, neglecting the shadowing effect of the net and the flow modification around the net cage. Li and Faltinsen (2012) studied theoretically the vertical responses of an isolated elastic, moored floater in regular waves. They pointed out that three-dimensional (3D) effects may cause important frequency-dependent hydrodynamic interactions at the scale of the floater. Kristiansen and Faltinsen (2012, 2015) studied experimentally and numerically a flexible-bottomless net cage attached to an elastic floater in waves and current. They showed that the elasticity of the floater was important for the mooring loads. In their work, the net cage was modeled by a truss model proposed by Marichal (2003), and the hydrodynamic forces on the cage were predicted by a screen model which accounts for hydrodynamic shadow and Reynolds number effect. They showed that their proposed hydrodynamic screen model gave reliable results even when the cage experienced large deformations which was not the case when Morison's equation was adopted. Their model was further adopted by He et al. (2015) to investigate the drag forces on a flexible-closed net cage in current and reasonable agreement between numerical and experimental results was achieved.

The fluid-structure interaction for the net cage is gaining increasingly more attention. Zhao et al. (2013), Bi et al. (2014a,b) and recently Yao et al. (2016) studied the flow inside and around a fish cage in current by solving the Navier-Stokes equation. The net was taken as a porous media with empirical coefficients. Both rigid and flexible cages were investigated. Their studies showed that numerical results would overestimate the hydrodynamic loads on the cage when compared with the experimental data if the effect of fluid-structure interaction was not considered. Although it maybe questionable to consider the net cage as porous media (most common practice), their work is valuable to show us the effect of considering the fluid-structure interaction.

In addition, a two-dimensional experimental study was carried out by Bardestani and Faltinsen (2013) with focus on snap loads due to independent motions of the floater and sinker tube when exposed to waves. They pointed out that the net experienced cyclic snap loads in higher wave amplitudes and periods which could also happen for full-scale offshore fish farms and should be of concern for the net design.

Few investigations are available for a realistic fish farm due to the complexity, but this kind of study is necessary to provide practical guidance for fish farm design. In the present paper we try to investigate the dynamic responses of a realistic floating collar fish farm system (with single cage) in both regular and irregular sea states and determine the survival conditions of the system. In order to deal with the problem, an efficient and reliable numerical solver is introduced at first. The curved beam equations with consideration of hydroelasticity introduced by Li et al. (2016) for an isolated elastic torus are adopted for the present two concentric floating tubes and also for the sinker tube. The net cage model proposed by Kristiansen and Faltinsen (2012) for a bottomless net cage is reliable and efficient, so it is adopted here for the closed net cage which comprises a cylindrical part and a conical part. The mooring lines are modeled as elastic trusses with correct weight and stiffness and Morison's equation is adopted to estimate the loads on the lines. Numerical results for a realistic fish farm system in both regular and irregular waves are compared with experimental data from Nygaard (2013). These model tests are further analyzed here using the numerical simulations as a complementary research tool. In particular, a sensitivity analysis is conducted to see what factors are important when modeling a realistic fish farm, especially what effects are dominant for the mooring loads. Finally, numerical simulations for fish farms with different set-ups are performed. Sea conditions are given according to the Norwegian standard StandardNorge (2009), from light exposure to heavy exposure, as

shown in Table 1. The main purpose is to check the survival conditions and the feasibility to move the conventional fish farms to more exposed regions.

In summary, the present paper is organized as follows. First, a description of the model tests conducted in Marintek (Nygaard, 2013) for a fish farm with realistic set-up is given in section 2. Next, numerical modelings of different components are briefly explained in section 3. Lastly, numerical results are compared with the experimental data for a realistic fish farm system in current only, wave only, combined waves and current and irregular seas, in section 4, along with a numerical sensitivity study where the effects of different parameters are discussed. Finally systematic simulations for fish farms with different set-ups are performed and the limitations of moving the conventional fish farm to more exposed regions are discussed.

Table 1: Environmental classification given in terms of significant wave height H_s, peak period T_p and current velocity U_∞ according to Norwegian Standard NS9415:2009. It is assumed irregular waves for each wave class. If regular wave is considered, the standard says that the corresponding wave height H can be assumed to be 1.9 times the significant wave height.

Wave	H_s(m)	T_p(s)	**Exposure**	**Current**	U_∞(m/s)	**Exposure**
A	0.0 - 0.5	0.0 - 2.0	Small	a	0.0 - 0.3	Small
B	0.5 - 1.0	1.6 - 3.2	Moderate	b	0.3 - 0.5	Moderate
C	1.0 - 2.0	2.5 - 5.1	Heavy	c	0.5 - 1.0	Heavy
D	2.0 - 3.0	4.0 - 6.7	High	d	1.0 - 1.5	High
E	>3.0	5.3 - 18.0	Extreme	e	>1.5	Extreme

2. Experiments

The model experiments for a realistic fish farm were carried out at the Ocean Basin Laboratory at MARINTEK, see Nygaard (2013). All measurements referred to hereinafter, relate to full-scale values, unless otherwise specifically indicated.

2.1. Model test set up

The physical model used in the experiments featured all the main components presented in a full-scale sea cage system (with single cage) commonly used in Norway, which included two concentric floating tubes, an elastic sinker tube, a cylindrical net cage with a conical bottom, mooring system comprising bridle lines, mooring frame lines, mooring buoys, coupling plates, chains connecting the coupling plates to the buoys and the anchor lines attaching the system to the bottom of the basin, see Figure 1. A model test scale of 1:16 was adopted and Froude scaling with geometric similarity except for the net twines was assumed. For the net twines, geometric similarity cannot be applied, as the net twine diameter and net E-module are too small to be realized in model scale if using geometric similarity. So nylon net twines were used in the model tests with correct solidity ratio of the net cage. Here the solidity ratio is defined as the ratio of the area of the solid part of a net screen to the total area of the screen. According to the screen model proposed by Kristiansen and Faltinsen (2012), the solidity ratio and the Reynolds number of the twines are two important parameters to estimate the drag force on the cage. Correct solidity ratio was used in the model test while the Reynolds number of the twine in model-scale (Re=100-300) is smaller than that in a full-scale cage (Re=500-1000). In terms of the drag coefficient of the twine, it is larger in model-scale ($C_D \approx$ 1.25-1.35) than that in full-scale ($C_D \approx$ 1.0-1.1). C_D is estimated according to the drag coefficient for a smooth circular cylinder. To represent a more realistic full-scale value, we should use as large twine diameter as possible in the model tests to keep the twine Reynolds number as high as possible. Two linear springs were inserted in the front two anchor lines where the forces were measured, as shown in the upper part of Figure 1. The sinker tube was attached directly to the net in present study, without vertical chains between the floating collar and the sinker tube to avoid chafing between the chain and the net cage. A list of relevant parameters and dimensions of the model-scale and corresponding full-scale values are given in Table 2 and Table 3. Photos illustrating the general set-up of different components are presented in Figure 2.

The instrumentation of the model consisted a total of 8 linear accelerometers, 14 force measurement devices, three wave gauges (one at the axis origin was used only for wave calibration, not in the model tests). Forces were measured in one bridle pair (bridle line-1 and bridle line-2) on the windward side of the floating collar; in the two front two anchor lines (anchor line-1 and anchor line-2); under two buoys (buoy-1 and buoy-2) in the 7 m long chain between the buoy and the coupling plate. Forces were measured in ropes connecting the sinker tube and the

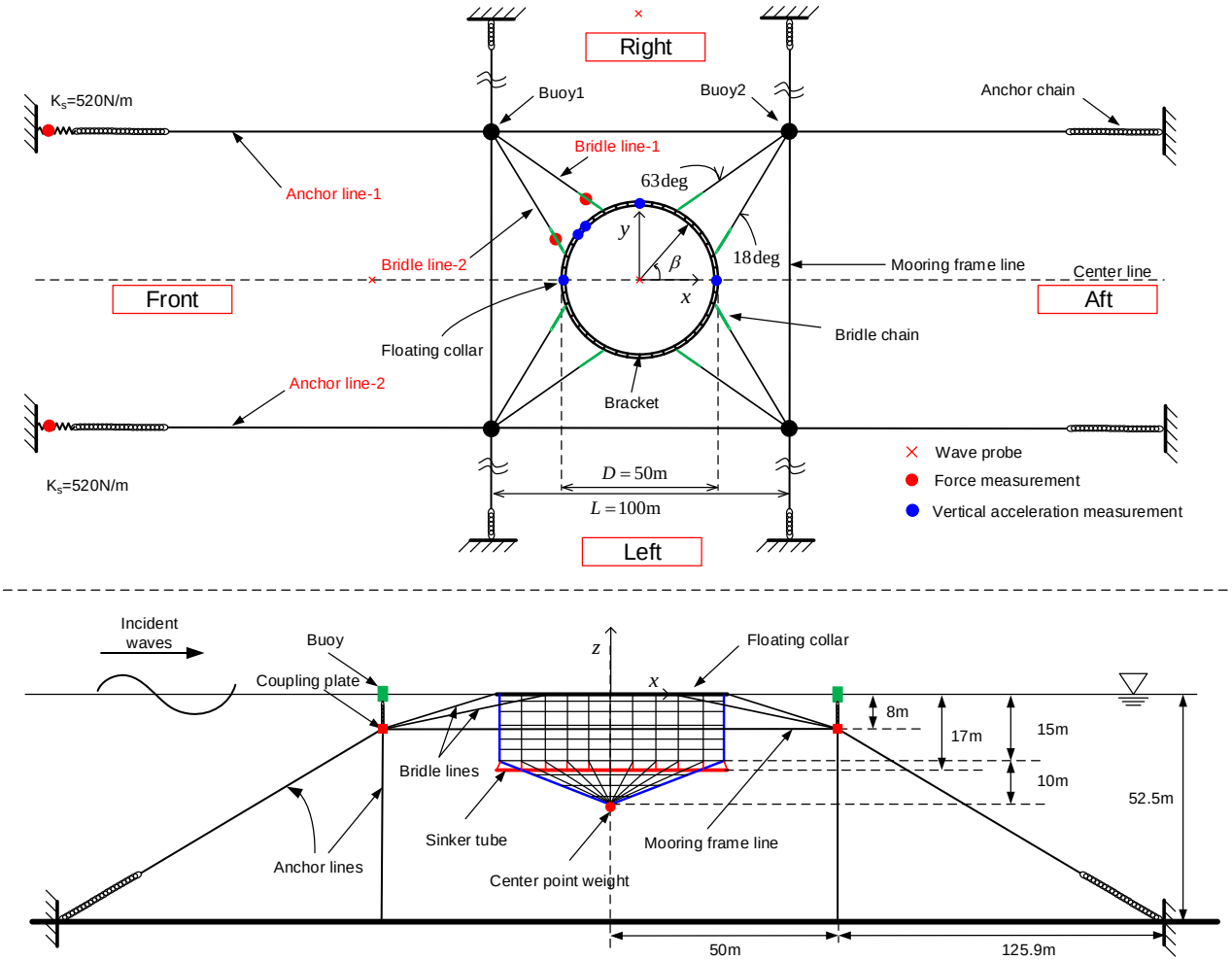

Figure 1: Experimental set-up (full-scale). Upper: top view. Lower: side view. Two springs were inserted in the front two anchor lines. The Cartesian coordinate system $oxyz$ is located at the center of the floating collar in calm conditions.

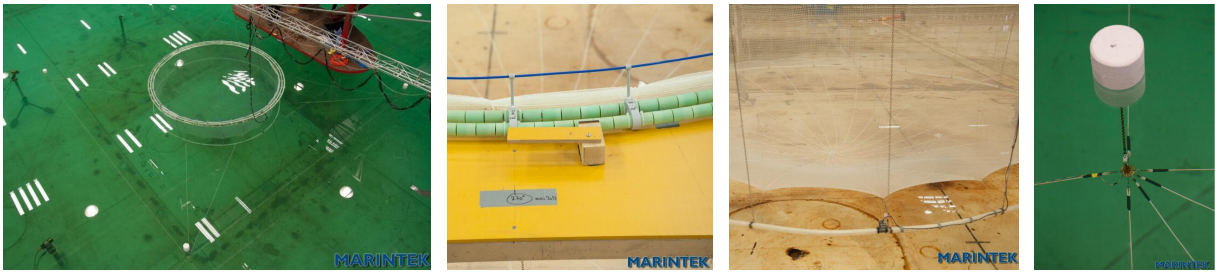

Figure 2: Photos of the physical set-up. Left: general set-up including the floating collar, the net cage, the sinker tube and the mooring system. Middle left: detail of the two concentric floating tubes which are combined by 40 brackets. Middle right: details of the sinker tube and the net cage. Right: photography showing the buoy, the coupling plate and the mooring lines.

net in positions with $\beta = 0$, $\pi/2$, $4\pi/5$, π, where β is defined in Figure 1. Forces were also measured in ropes in the net cage, about 5 m down from the floating collar with $\beta = 0$, $\pi/2$, $4\pi/5$, π. The positions of the majority of the instruments are shown in Figure 1.

Table 2: Parameters of the floating collar, net cage and sinker tube in the model tests. Both model-scale (MS) and full-scale values (FS) are given. Since 'ordinary' nylon ropes were used for the net cage in the model tests, the corresponding full-scale E-module (E_{net}) is larger than that used in full-scale cages. The parameters marked with * are not presented in Nygaard (2013) and are from a similar experiment.

Description	**Symbol**	**Model scale**	**Full scale**	**Unit**
Floating collar				
Number of tubes	-	2	2	-
Diameter inner tube (center)	D_{f1}	3.125	50	m
Diameter outer tube (center)	D_{f2}	3.2375	51.8	m
Distance between tubes	p	56.25	900	mm
Tube section diameter	d_f	28.125	450	mm
Tube bending stiffness	EI_f	0.72	7.72×10^5	Nm^2
Tube mass	m_f	0.124	32.54	kg/m
Net cage				
Diameter	D_c	3.125	50	m
Depth of vertical net	h_u	0.9375	15	m
Depth of cone net	h_l	0.625	10	m
Net twine diameter*	d_w	0.975	3.25	mm
Net mesh-bar length*	l_w	7.5	14.3	mm
Net E-module*	E_{net}	5×10^8	8.2×10^9	N/m^2
Net solidity	Sn	0.26	0.26	-
Center point weight	W_c	0.048	200	kg
Sinker tube				
Tube diameter	D_s	3.2375	51.8	m
Tube section diameter	d_s	17.5	280	mm
Tube depth	h_s	1.0625	17	m
Tube bending stiffness	EI_s	0.195	2.0×10^5	Nm^2
Mass per meter in water	w_s	0.095/0.191	25/50	kg/m

2.2. The models

The floating collar composed of two floating tubes with outer cross-sectional diameter $d_f = 2c_f$=450 mm. Selected SDR (SDR=diameter/wall thickness) was 17.6, i.e. the wall thickness of the plastic tube was 25.6 mm. Floating tubes were modeled with correct outer diameter, horizontal circumference, buoyancy and bending stiffness. The diameter of the center line of the inner tube was D_{f1}=50 m. The outer tube was positioned with a pipe diameter distance (center-to-center distance p=0.9 m) outside the innermost, leading to the center line diameter D_{f2}=51.8 m. The tubes were held together by 40 brackets. The specific fluidity of each of the tubes was 0.2, i.e. the dry weight in relation to the buoyancy of fully submerged pipe, leading to the mass per unit length of the tube m_f=32.54 kg/m. Bending stiffness of the tubes was Froude scaled in the model tests to have correct elastic natural frequencies for both horizontal and vertical modes. The bending stiffness (full scale) of each of the tube was EI_f=7.715×10^5 Nm^2.

A sinker tube with center line diameter D_s=51.8 m, cross-sectional diameter $d_s = 2c_s$=280 mm and bending stiffness EI_s=2.0×10^5 Nm^2 was chosen. Two different submerged masses were adopted with w_s=25 kg/m and 50 kg/m. A center point weight with W_c=200 kg submerged mass was attached to the lower end of the net, see Figure 1.

A cylindrical net cage with a conical bottom was attached to the floating collar with net-height of the cylindrical part h_u=15 m and conical part h_l=10 m and a typical solidity ratio Sn=0.26. In the lower edge of the cylindrical part 20 ropes were attached to connect the sinker tube.

The anchor system, consisting of a square 100 m × 100 m frame anchoring, was laid out around the net 8 m deep and was held in place by 4 buoys, one buoy at each corner. At each spar buoy hangs a 7 m long chain, where the lower end was attached to a steel plate. From each steel plate went there 2 bridle lines into the floating collar and two anchor lines down to the bottom. Bottom depth was set to 52.5 m.

Table 3: Parameters of the mooring system in the model test. The springs were inserted in the lower end close to the anchor in the front two mooring lines, as shown in Figure 1. The stiffness of the anchor lines without spring were 2180N/m, inserted spring stiffness k_s was 520 N/m, giving a total line stiffness of about 420 N/m, as was the specified value. All values given above are in model scale. The full-scale stiffness of the bridle lines and frame lines are larger than those used in commercial full-scale cages, since 'ordinary' ropes were used in the experiments. All ropes were almost without weight in water and were intended to provide just geometry contribution. The parameters marked with * are not presented in Nygaard (2013) and are from a similar experiment.

Description	**Model scale**	**Full scale**	**Unit**
Bridle lines			
Position on cage (bridle-1)	117	117	degree
Position on cage (bridle-2)	162	162	degree
Bridle rope diameter*	2.5	40	mm
Bridle chain diameter*	1.4	22.4	mm
Bridle chain length *	0.342	5.47	m
Bridle chain mass *	0.033	8.66	kg/m
Bridle stiffness *	1.85	486.1	kN/m
Frame lines			
Mooring frame length	6.25	100	m
Mooring frame depth	0.5	8	m
Frame rope diameter*	3.2	51.2	mm
Frame stiffness*	3.92	1.03×10^3	kN/m
Anchor lines			
Anchor line length	8.344	133.5	m
Anchor rope length*	6.47	103.5	m
Anchor rope diameter*	3.2	51.2	mm
Anchor chain length*	1.88	30	m
Anchor chain diameter*	2	32	mm
Anchor chain mass*	0.061	16.0	kg/m
Anchor line stiffness (no spring)	2.18	572.0	kN/m
Anchor line stiffness (with spring)	0.42	110.2	kN/m
Buoys system			
Number of buoys (1 at each corner)	4	4	-
Buoy diameter *	0.0965	1.55	m
Buoy length*	0.146	2.34	m
Buoy mass*	0.035	146.9	kg
Buoy Chain length	0.4375	7	m
Buoy chain mass*	0.033	8.66	kg/m
Buoy chain diameter*	1.4	22.4	mm
Coupling plate mass	0.013	55	kg

2.3. Test conditions

A total of 6 irregular waves (long crested), 4 regular waves and two current only cases were considered in the present study. The test matrix is presented in Table 4. The same test number used in Nygaard (2013) is adopted in the present paper. The 6 irregular waves were generated according to the definition of JONSWAP wave spectrum with spectrum peakedness γ=2. All wave spectra were generated corresponds to 1.5 hour (full-scale) duration. The measured values at the given sea states have less than 5% deviation from specified values with respect to the significant wave height H_s and peak wave period T_p. The actual current speed in the facility was found to be 0.48 $\pm$ 0.031 m/s and 0.72 $\pm$ 0.046 m/s when specified to be 0.5 m/s and 0.7 m/s, respectively.

2.4. Pretension

In order to benchmark numerical results with experimental data, we should know the pretension forces of the system in static configuration. The original report does not present the values of the pretension forces, instead we obtain the pretension forces from the time histories of the mooring loads in static condition. Results from model

Table 4: Test matrix showing prototype (full) scale current velocity, wave height and wave period (regular wave) and significant wave height and peak wave period (irregular wave). CUR, REG and IRR represent current, regular and irregular waves. BR represents mass per unit length of the sinker tube.

Test no.	**Test type**	H_s(m)	T_p(s)	**Current** U_∞(m/s)	**Comments**
5010	CUR	-	-	0.5	BR=50 kg/m
5020	CUR	-	-	0.7	BR=25 kg/m
5030	IRR	1.0	4.0	0.5	BR=50 kg/m
5040	IRR	1.5	4.5	0.5	BR=50 kg/m
5050	IRR	2.0	5.0	0.5	BR=50 kg/m
5060	IRR	2.5	6.0	0.5	BR=50 kg/m
5070	IRR	3.0	7.0	0.5	BR=50 kg/m
5080	IRR	4.0	8.0	0.5	BR=50 kg/m
5150	REG	2.5	6.0	-	BR=50 kg/m
5160	REG	2.5	8.0	-	BR=50 kg/m
5170	REG	2.5	6.0	0.5	BR=50 kg/m
5180	REG	2.5	8.0	0.5	BR=50 kg/m

tests show that mean pretension forces (full scale) in anchor line-1 and anchor line-2 are 38.4 kN and 25.3 kN, respectively, which means that the model has asymmetric pretension forces.

3. Theory and numerical model

In this section, we will first give an introduction of theories for generating both regular and irregular waves. Then we will describe in some detail the theoretical models for different components of a realistic fish farm system including the floating collar, sinker tube, net cage and mooring system. Numerical models for the different components are carefully validated by experimental data for simplified fish farms. The comparisons are not shown here as the focus is on a complete fish-farm system.

3.1. Wave field

The responses of a fish farm system in both regular and irregular waves are to be investigated. Linear potential wave theory is adopted to describe the regular waves. According to Faltinsen (1990), the deep-water wave potential φ_0 for a wave propagating along the positive x-axis is given as

$$\varphi_0 = \mathrm{Re}\left\{\frac{ig\zeta_a}{\omega}e^{-i(kx-\omega t)}e^{kz}\right\} \tag{1}$$

where Re denotes real part of a complex value, i is the imaginary unit, t the time, ζ_a the wave amplitude, g the gravitational acceleration, ω the circular frequency and $k = \omega^2/g$ the wave number. The corresponding wave elevation according to linear wave theory is

$$\zeta(x,t) = \zeta_a \cos(kx - \omega t) \tag{2}$$

From the amplitude spectrum estimated from the time history of generated regular wave in the experiment, small contribution from double frequency 2ω component is observed. So second-order Stokes waves theory is also considered in the sensitivity analysis when estimating the hydrodynamic forces on the net cage.

For long crested irregular waves, the surface elevation $\zeta(x,t)$ at a position x and time t is obtained as the superposition of multiple (N) monochromatic waves

$$\zeta(x,t) = \sum_{i=1}^{N} A_i \cos(k_i x - \omega_i t + \varepsilon_i) \tag{3}$$

where A_i is the amplitude of the wave associated with the circular frequency ω_i and $k_i = \omega_i^2/g$ is the corresponding wave number. ε_i is the random phase angle for frequency component i and is uniformly distributed between 0 and 2π. The wave amplitude A_i is given as

$$A_i = \sqrt{2S(f_i)\Delta f} \tag{4}$$

where $S(f)$ is the wave spectrum, $f_i = \omega_i/2\pi$ is the wave frequency . Δf is the frequency interval. If a constant frequency interval is used, the realization of the wave elevation with respect to time will not be a real random process. The wave elevation will have a return period $T_r = 1/\Delta f$, which means that the wave pattern will repeat for each time period T_r. So small constant Δf is needed for long time simulation. The solution is random frequency intervals for each f_i. We can obtain random frequency seed $f_i^{'}$ by

$$f_i^{'} = f_i + \Delta f p_i \tag{5}$$

where f_i is obtained with constant frequency interval Δf, p_i is a random stochastic variable evenly distributed between -0.5 and 0.5. In terms of the wave spectrum, the JONSWAP wave spectrum was used in the experiment and defined as

$$S(f) = \alpha g^2 (2\pi)^{-4} f^{-5} \exp(A)\, \gamma^{\exp(B)} \tag{6}$$

Here $A = -1.25(f/f_p)^{-4}$, $B = -(f-f_p)^2/\left(2\sigma^2 f_p^2\right)$, $\alpha = 5.061 H_s^2 f_p^4 (1.0 - 0.287 \ln\gamma)$, f is the frequency in [Hz], $f_p = 1/T_p$ frequency of spectral peak in [Hz], σ the spectral width parameter =0.07 for $f < f_p$ and =0.09 for $f > f_p$, H_s the significant wave height, γ the spectral peakedness. A sample of the wave spectrum derived from generated irregular wave in the experiment and that given according to the JONSWAP wave spectrum with significant wave height H_s= 4m, peak wave periods T_p =8s and spectrum peakedness γ=2 is shown in Figure 3.

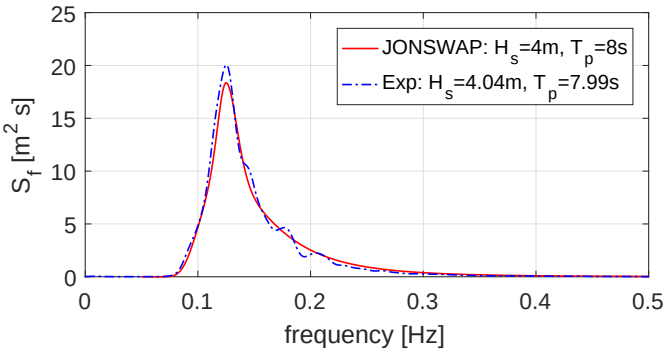

Figure 3: Comparison of the wave spectrum from the experiment and from the theory with significant wave height H_s= 4 m and peak period T_p = 8 s.

3.2. The floating collar

In this section we give a brief introduction of the structural model and hydrodynamic-load model for the floating collar. The floating collar comprises two floating tubes and is assumed to be circular in calm water and the motions, (x_f, y_f, z_f), are assumed to be a combination with rigid-body motions as well as elastic perturbations around the original circular shape in lateral (radial) and vertical directions. The Earth-fixed coordinate system $Oxyz$ is shown in Figure 1. The vertical z-axis coincides with the tube axis at rest, is positive upwards, and zero in the mean water line. The current and waves are assumed to be along the positive x-axis, which implies that only modes symmetric about the x-axis are excited. The vertical (z_f) and radial (v_f) displacements are expressed by the following Fourier series

$$\begin{aligned} z_f(\beta, t) &= a_0(t) + \sum_{n=1}^{\infty} a_n(t)\cos(n\beta) \\ v_f(\beta, t) &= \sum_{n=1}^{\infty} b_n(t)\cos(n\beta) \end{aligned} \tag{7}$$

Here β is the radial angle along the tube with β=0 corresponding to the x-axis, as defined in Figure 1. The coefficient a_0 represents the heave motion, $a_1 \cos\beta$ is the vertical motion due to pitch involving a coupling between rigid-body and elastic motions and $a_n \cos n\beta$ ($n \geq 2$) are purely vertical elastic modes. The coefficients b_n ($n \geq 2$) are connected with the horizontal elastic radial mode n and $b_1 \cos\beta$ is due to the rigid-body surge motion. The motion equations for the floating collar can be solved in a similar way as that proposed by Li et al. (2016) for an elastic floating torus, based on a curved beam equation that accounts for axial tension and curvature effects. The equation for the vertical motion is

$$m\frac{\partial^2 z_f}{\partial t^2} + EI\left(\frac{\partial^4 z_f}{\partial s^4} + \frac{1}{R^2}\frac{\partial^2 z_f}{\partial s^2}\right) - \frac{\partial}{\partial s}\left(T_{ax}\frac{\partial z_f}{\partial s}\right) = f_z\left(s,t\right) \tag{8}$$

where $m = 2m_f$ [kg/m] is the mass per unit length for two tubes, $R = (D_{f1}/2 + D_{f2}/2)/2$ the mean value of the center line radius of the two tubes, t the time variable, s the curvilinear coordinate along the floating collar, $EI = 2EI_f$ the structural bending stiffness for two floating tubes, $\partial/\partial s$ the differentiation along the floating collar and T_{ax} the steady axial tension along the floating collar. f_z is the vertical forces per unit length, including wave excitation forces, added mass and damping forces, restoring forces, forces from the net cage, mooring lines and drag force on the tubes. The axial tension T_{ax} is estimated by a two-dimensional Finite Element Method (FEM) code. A comparison of the axial tensions by FEM and by a simplified analytical method proposed in Kristiansen and Faltinsen (2015) is performed and satisfactory agreement is achieved. The advantage of using the FEM is that one can estimate the variation of the tension along the floating collar. Substituting Eq. (7) into Eq. (8), then multiplied by $\cos n\beta$ and integrated from $\beta = 0$ to 2π, we can have the decoupled motion equations for different vertical modes. For detailed expressions, interested readers can refer to Li and Faltinsen (2012) and Kristiansen and Faltinsen (2015). One thing to be mentioned is that we express the hydrodynamic radiation loads for different modes in terms of convolution integrals with retardation functions according to linear potential-flow theory, neglecting the influence of current, so the transient responses of the floating collar can be considered. Similar equations are obtained for horizontal modes and are omitted here. Curved beam equations are also applied to the sinker tube and the hydrodynamic loads are calculated by the modified Morison's equation.

3.2.1. Drag on the floating collar

Viscous load on the floating collar is moderate compared with the total force on the system, so it is not necessary to estimate the load by accurate yet time-comsuming method, as done by Kristiansen (2010) for a horizontal cylinder in waves using a computational Computational Fluid Dynamics (CFD) method. Here we apply the drag term in Morison's equation to model the drag force per unit length on a tube in the horizontal plane, given by

$$f_r^{\text{drag}}\left(\beta,t\right) = 0.5\rho C_D^f d_r u_r \left|u_r\right| \tag{9}$$

where C_D^f is the drag coefficient , $d_r\left(\beta,t\right) = \min\left(\zeta - z_f + c_f, 2c_f\right)$ is the relative submergence, neglecting the radiation and diffraction waves in the free surface elevation, $u_r(\beta,t) = \mathbf{U}_{\text{rel}} \cdot \mathbf{n}_f$ is the local, relative cross-flow velocity at the center line of the tube with $\mathbf{U}_{\text{rel}}$ the instantaneous, relative velocity vector between the undisturbed inflow and the floating collar and $\mathbf{n}_f = (\cos\beta, \sin\beta, 0)$ the two-dimensional (in the horizontal plane) unit normal vector of the tube when undeformed (circular shape).

The next step is to find the drag coefficients C_D^f for different cross-sections which is not straightforward. The cross-sections of the floating collar will experience different inflow because the waves and current are not in general aligned with the cross-section. For a given cross-section with cross-flow, it can be seen as two circular cylinders in tandem arrangement. The flow interaction is important as the downstream cylinder is located in the wake of the upstream cylinder. According to the results from Zdravkovich (1985) for two fully submerged circular cylinders in current, drag coefficients for the upstream and downstream cylinders are strongly dependent on the Reynolds number and the distance between the two cylinders. Drag coefficient can even be negative for the second cylinder when the two cylinders are placed close enough (center-to-center distance $p < 4d_f$, d_f is the cross-sectional diameter of the tube). In the presence of incident waves, over-topping of the floating collar may occur when it is exposed to steep waves and also the drag coefficient C_D^f depends on the Keulegan-Carpenter number (KC) as well as the ratio between the wave particle amplitude and current velocities in the case of combined waves and current. So it is not practical to account for all these variations of C_D^f. In the present study, constant drag coefficients for the two cylinders are assumed with $C_{D,1}^f = 1.0$ and $C_{D,2}^f = 0.0$, according to Zdravkovich (1985) for two cylinders in current with relative distance $p/d_f = 2$ (used in our study), neglecting the influence of Reynolds number. The sensitivity of the mooring loads to the drag force of the floating collar is studied in section 4.

3.2.2. Forces on the sinker tube

The radial f_r and vertical f_z forces per unit length on the sinker tube are calculated by the modified Morison's equation for a submerged circular cylinder, i.e.

$$\begin{aligned} f_r &= 0.5\rho C_D^s d_s u_r \sqrt{u_r^2+u_z^2} + C_M^s \rho\pi \tfrac{d_s^2}{4}\ddot{r}_w - (C_M^s-1)\rho\pi\tfrac{d_s^2}{4}\ddot{v}_r \\ f_z &= 0.5\rho C_D^s d_s u_z \sqrt{u_r^2+u_z^2} + C_M^s \rho\pi \tfrac{d_s^2}{4}\ddot{z}_w - (C_M^s-1)\rho\pi\tfrac{d_s^2}{4}\ddot{z}_r \end{aligned} \tag{10}$$

Here d_s is the cross-sectional diameter of the sinker tube; u_r and u_z are the local, radial and vertical relative cross-flow velocity between the sinker tube and ambient flow, evaluated at the center axis of the sinker tube; $\ddot{v}_r$ and $\ddot{z}_r$ are the radial and vertical accelerations of the sinker tube; $\ddot{r}_w$ and $\ddot{z}_w$ the radial and vertical undisturbed wave particle accelerations at the center axis of the sinker tube; C_D^s and C_M^s are the drag and mass coefficients. The main parameters affecting C_D^s and C_M^s are the Keulegan-Karpenter number KC, Reynolds number Re and the relative current number. In our case, the sinker tube operates at small KC number, so we approximately set $C_M^s = 2$ according to low values of KC number. $C_D^s = 1$ is assumed, neglecting the influence of oscillatory ambient flow and Reynolds number.

3.3. The net cage

In this section we describe the structure model for the net cage and the hydrodynamic model for the viscous load on the net cage.

3.3.1. Truss model

The structural model of the net cage from Kristiansen and Faltinsen (2012, 2015), originally presented by Marichal (2003), is adopted in the present paper. The mesh wires of the net cage are modeled as linear elastic trusses. Viscous loads exerted on the cage are transferred to the nodes of these trusses. Once the hydrodynamic loads acting on each node are known, the kinematic constraint of each twine leads to a linear equations system of the truss tensions. Then the whole system is evolved accordingly after obtaining the unknown truss tensions. The main particular of this truss model is that a linear system of equations for the truss tensions is implicitly solved each time-step.

3.3.2. Hydrodynamic screen model

The screen type force model proposed by Kristiansen and Faltinsen (2012, 2015) is adopted in present paper to estimate the hydrodynamic, viscous force acting on the net cage. They demonstrated that the screen type force model gave clear improvements in predicting the drag and lift forces on the net cages relative to those predicted by a Morison type of force model, especially when the net cage is subjected to large deformations. Just a brief outline of the screen force model is given here.

In the screen model, the net cage is divided into net panels, see Figure 4. Each net panel is assumed to experience a viscous normal force due a pressure drop proportional to the local, relative flow velocity squared, and a tangential force due to that the flow is deflected when going through the net. The instantaneous, relative flow velocity $\mathbf{U}_{\text{rel}}$ is taken as

$$\mathbf{U}_{\text{rel}} = \gamma\mathbf{U}_\infty + \mathbf{u}_w - \mathbf{u}_j \tag{11}$$

where $\mathbf{U}_\infty$ is the ambient current velocity, $\mathbf{u}_w$ the water particle velocity at the position of the node, and $\mathbf{u}_j$ is the velocity of the node. $\gamma = 1$ in the front part of the net, while $\gamma = r$ in the rear half the net, accounting for the shading effect of the front part net. r is a flow reduction coefficient and estimated according to Løland (1991). it is assumed that only the steady part of the flow, i.e. the current, that is reduced by r.

The normal and tangential viscous forces are assumed to be functions of Sn, Re and θ, where Sn is the solidity ratio of the net, Re is the Reynolds number and θ is the angle between the panel normal vector and the local flow velocity, as shown in Figure 4. The Reynolds number used by Kristiansen and Faltinsen (2015) was defined as: Re= $(\gamma U_\infty + u_{wa})d_w/(1\text{-Sn})\nu$, where d_w is the physical twine diameter of the net, u_{wa} is velocity amplitude of an undisturbed water particle at the at the initial position of the net node and ν is the kinematic viscosity of the water. Their main argument was that the Reynolds number should be defined by the characteristic free stream velocity. However, their definition may be difficult to implement in irregular sea scenario. So here the Reynolds number is defined as: Re= $|\mathbf{U}_{\text{rel}}|\, d_w/(1\text{-Sn})\nu$, using the instantaneous relative velocity instead of the characteristic free stream velocity . Numerical simulations indicate that the difference of the viscous loads on the net cage in waves and current is small when the two definitions are adopted, respectively.

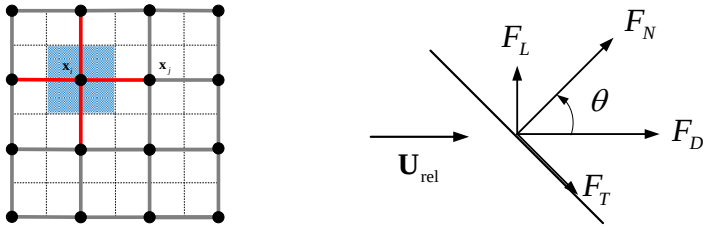

Figure 4: Left: Division of a planar net into an equivalent truss model. The solid black circles denote the nodes. The shaded areas represent the net panels surrounding a given node and are used to estimate the hydrodynamic forces acting on the node. The red lines represent the equivalent trusses with two end nodes. Right: Drag (F_D) and lift (F_L) forces on a net panel. F_N and F_T denotes the corresponding normal and tangential components. The angle θ is the angle between the normal of the panel and direction of local inflow with velocity $\mathbf{U}_{\text{rel}}$.

3.4. The mooring system

The set-up of the mooring system is shown in Figure 1, which typically comprises ropes and chains, with buoys to support all mooring lines. Ropes and chains are treated in a similar way as the net and are modeled as elastic trusses with correct diameter, weight and stiffness. The hydrodynamic forces on the mooring lines are estimated by modified Morison's equation based on the cross-flow principle and by neglecting the longitudinal forces. The buoys are floating circular cylinders and the motions are solved in an inertial coordinate system. Because the considered wavelengths are long relative to the buoy diameter, long wave approximation is adopted. There are assumed no coupling terms between the translational and rotational motions as pressure loads are dominant. As an example, the equation for surge motion is

$$M_B\ddot{\eta}_1 = F_{1,B}^{\text{Excit}} + F_{1,B}^{\text{Added mass}} + F_{1,B}^{\text{Visc}} + F_{1,B}^{\text{Ext}} \tag{12}$$

where M_B is the buoy mass, $F_{1,B}^{\text{Excit}}$, $F_{1,B}^{\text{Added mass}}$, $F_{1,B}^{\text{Visc}}$, $F_{1,B}^{\text{Ext}}$ are the wave potential-flow excitation force including Froude-Kriloff force and diffraction force, added mass force, viscous force and external force from the chain under the buoy, exerted in the surge direction. The excitation force, added mass force and viscous force are estimated by the modified Morison's equation and the corresponding drag coefficient C_D^B and mass coefficient C_M^B are assumed to be constant for simplicity with C_D^B=1 and C_M^B=2.0. The sensitivity of the mooring loads to the drag and mass coefficients of the buoy is investigated in section 4.

4. Results with numerical sensitivity analysis

In this section, we present results from the numerical simulations and the experiments for the realistic fish farm system introduced in section 2. The main focus is on the mooring loads in the front two anchor lines and bridle lines. Nominal results from cases in current only are presented in section 4.1. "Nominal" denotes that basis values of different parameters are used in the simulations. A detailed sensitivity analysis is also presented. Nominal results from cases in waves only and combined waves and current are presented and discussed in section 4.2, together with a sensitivity analysis. Numerical and experimental results for the system in irregular waves are shown in section 4.3. Finally systematic simulations of fish farms with different set-ups in different exposure scenarios are performed in section 4.4 to identify the operational limits of the conventional fish farm system.

4.1. Current only

In this section, we present the results of the mooring loads in the front two anchor lines for cases in current only. We will focus on the average value of the loads in the front two anchor lines (anchor load). Numerical results are compared with the experimental data. Nominal results with a convergence study are shown at first, then a detailed sensitivity analysis is presented, identifying the dominant parameters influencing the anchor loads.

4.1.1. Nominal results

A convergence study for cases in current only was performed at first and three different meshes were tested. Steady shapes of the net with different mesh resolutions are presented in Figure 5. Numerical results indicate that the anchor load is not sensitive to the mesh and a relative coarse mesh is enough to reach convergence. The mesh $N_H \times N_V = 20 \times (8{+}6)$ is adopted as the nominal mesh and to be used in the sensitivity analysis. A comparison of the anchor line loads between numerical and experimental results is given in Figure 6. Two different sinker tube weights are considered. From the figure we can have the following conclusions: (1) increasing the weight of the sinker tube does not have significant influence on the anchor load for low current velocities, but has more effect for higher current velocities. The main reason is that the projected area of the net cage in the current direction is important for the anchor load and it is influenced by sinker tube weight and current velocity U_∞; (2) numerical results slightly over-predict the anchor loads compared to the experimental data, especially for the case with smaller current velocity and higher sinker tube weights. One of the possible reasons is that the flow around the net cage due to the presence of the net cage is not considered. It is assumed that all the water goes through the net cage in nominal simulations.

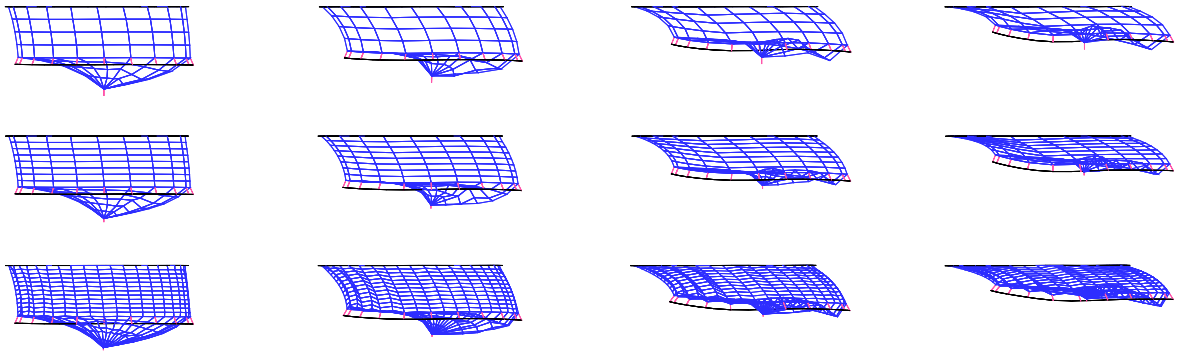

Figure 5: Steady-state shapes of a realistic fish farm system (mooring system not shown): convergence study. The weight of the sinker tube is 50kg/m. From top to bottom: $N_H \times N_V = 20 \times (4+4)$, $20 \times (8+6)$ and $40 \times (12+6)$. N_H and N_V denote the number of trusses in the horizontal and vertical directions. N_V comprises two parts: meshes for cylindrical and conical part. From left to right: $U_\infty = 0.2$, 0.4, 0.6, and 0.8 m/s.

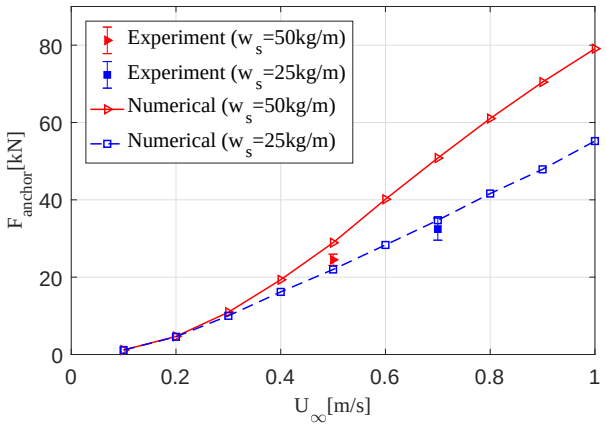

Figure 6: Average value of the loads in the front two anchor lines. Pretension force is subtracted. Filled symbols with error bar: experimental results. Red triangular symbol for case 5010 with current velocity 0.5 m/s and sinker tube weight 50 kg/m. Blue square symbol for case 5020 with current velocity 0.7 m/s and sinker tube weight 25 kg/m. Solid line and dashed line: present simulations with sinker tube weight equals 50 kg/m and 25 kg/m, respectively.

4.1.2. Numerical sensitivity analysis

Due to uncertainties in the experiments and lack in the information required to complete the mathematical modeling, we performed a sensitivity analysis. The different parameters examined are shown in Table 5. The

parameters are given separately for different components. Some parameters given in the table are relevant only for cases with waves and are not investigated here. In order to quantify the significance of the different parameters and try to identify important ones, we present condensed results in Figure 7 and 8. Two sinker tube weights are investigated. In Figure 7, each bar represents the percentage difference of the anchor force with respect to the nominal value, averaged over all the current velocities. Here the anchor force means the average value of the tensions in the front two anchor lines. As seen from the figure, each parameter has different impact on the anchor force.

Table 5: Parameters that are varied in the sensitivity analysis of anchor force for cases in current only, waves only and combined waves and current. Quantities with subscript 0 means nominal values, as given in Table 2 and Table 3. $a_{33}^n(0)$ means zero frequency added mass coefficients for the floating collar (No. 3). Nominal number of vertical and radial modes for both the floating collar (No. 6) and the sinker tube (No. 10) are $N_v = N_h = 8$. The flow modification around the net cage is not considered in nominal simulations (No. 12). Nominal weight of the net in water is zero (No. 13). Mean pretension denotes that the average value of the pretension forces in the front two anchor lines is adopted (No. 24). Parameters that impose more than 5% difference from nominal value are marked by "×" in the right three columns. Parameters not investigated are marked by "-".

	No.		Explanation	>5%		
				Current	Wave	Waves and current
Wave	1	Second-order wave	Wave theory	-		
Floating collar	2	Nonlinear FK + rest	Froude Kriloff force	-		
	3	$a_{33}^n(0)$	Added mass	-		
	4	$T_{ax} = 0$	Axial stiffness	-		
	5	$C_{D,1}^f$=0, $C_{D,2}^f$=0	Drag force			×
	6	N_h=1, N_v=2	Rigid body motions			
Sinker tube	7	C_D^s=0	Drag force			
	8	$w_s = 0.9w_{s,0}$	Weight in water			
	9	$w_s = 1.1w_{s,0}$	Weight in water			
	10	N_h=1, N_v=2	Rigid body motions		×	
Net	11	r= 0	Flow reduction factor	×	-	×
	12	-	Flow around net cage	-	-	-
	13	m_{net}= $1.1m_{\text{net},0}$	Mass of net	×		
	14	L_u= $0.9L_{u,0}$	Net depth (cylindrical)	×		
	15	L_u= $1.1L_{u,0}$	Net depth (cylindrical)	×		
	16	D_C= $0.9D_{C,0}$	Diameter (conical part)	×		
	17	D_C= $1.1D_{C,0}$	Diameter (conical part)	×		×
	18	E_{net}=$6.25 \times 10^7 N/m^2$	E-modulus of net twines			
	19	E_{net}=$5 \times 10^{10} N/m^2$	E-modulus of net twines			
	20	Sn=0.9Sn_0	Solidity ratio of net cage	×		×
	21	Sn=1.1Sn_0	Solidity ratio of net cage	×		×
	22	W_c=$0.9W_{c,0}$	Center point weight			
	23	W_c=$1.1W_{c,0}$	Center point weight			
Moorings	24	Mean pretension	Pretension moorings			
	25	$k_s = 0.9k_{s,0}$	Spring stiffness moorings			
	26	$k_s = 1.1k_{s,0}$	Spring stiffness moorings			
	27	$m_{\text{chain}} = 0.9m_{\text{chain},0}$	Anchor chain mass			
	28	$m_{\text{chain}} = 1.1m_{\text{chain},0}$	Anchor chain mass			
	29	C_D^B=0	Buoy drag coefficient			
	30	D_B=$0.9D_{B,0}$	Buoy diameter	-	×	
	31	D_B=$1.1D_{B,0}$	Buoy diameter	-	×	

Parameters with more than 5% difference with respect to nominal values are marked by "×" in the third last column in Table 5 for cases in current only, waves only and combined waves and current. In this section, we will just discuss results for current only cases. The rest are explained in section 4.2.2. Parameters not considered are marked by "-". One general observation is that the anchor force is more sensitive to the modeling of the net cage than other components. More detailed discussions are presented in the following:

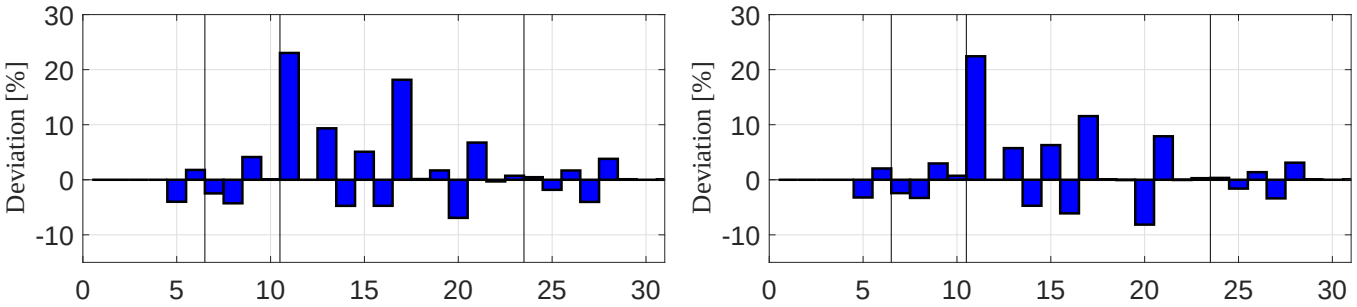

Figure 7: Each bar represents the percentage difference of the anchor force with respect to the nominal value, averaged over all the current velocities. The numbers on the horizontal axis refer to variation number as given in Table 5. Left: sinker tube with weight 25 kg/m. Right: sinker tube with weight 50 kg/m.

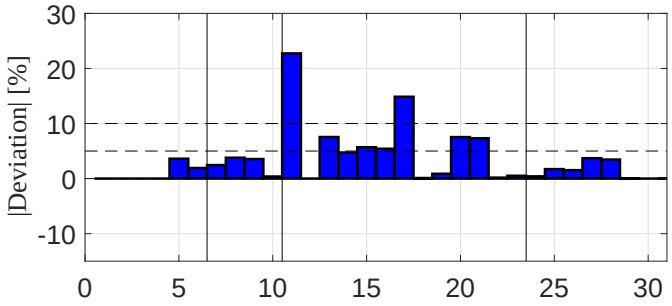

Figure 8: The mean of the absolute value of the condensed data presented in Figure 7.

Floating collar and sinker tube: When the drag forces on the two floating tubes are neglected, namely drag coefficients $C^f_{D,1}$=0, $C^f_{D,2}=0$ for the two tubes, the anchor force has a 4% reduction which means that the drag on the floating collar is quite moderate compared with the total drag on the system. So it is not necessary to model the drag force on the floating collar in a very accurate and time-consuming way. Modeling the floating collar as a rigid body has a small effect on the anchor force. Similar conclusions are obtained for the sinker tube.

Net cage: The flow reduction factor r in the rear part of the net cage due to the shadowing effect is the most important parameter for the anchor force and the anchor force will increase up to 22% if the shading effect is neglected. The flow around the net cage due to the presence of the net cage is not considered in nominal simulations and could be one of the possible reasons that numerical results tend to overestimate the drag forces on the cage. However there is no easy way to have a reliable prediction of the flow, so it is not investigated in the sensitivity analysis. The weight of the net in water is assumed to be zero in nominal simulations, so the weight of the net equals the buoyancy of the net. Archimedes' principle is directly applied to estimate the net buoyancy which maybe problematic since the net is not completely surrounded by water. The weight of the net in water is slightly larger than zero in reality. Increasing the net weight by 10% in the sensitivity analysis changes the anchor load by about 7%. Detailed variation of the structural modeling of the net is also considered. Changing the net depth (cylindrical part) and the net solidity ratio by 10% lead to a similar deviation from the nominal value by about 5% to 7%. Increasing the net diameter (conical part) by 10% will lead to larger deviation, about 15%. This is due to a big increase of the net volume, consequently larger drag force on the net. The effect of the net elasticity is also investigated. Ordinary ropes were used in the model test for the net cage, however when scaled up using Froude-scaling, the elasticity gives higher stiffness than for net used in commercial full-scale cages. A model scale Young's modulus of E_{net}=$6.25 \times 10^7 N/m^2$ would conform more to a realistic full-scale value, but could be difficult to realize in a model test set-up. So two different net elasticities are tried in the sensitivity analysis with E_{net}=$6.25 \times 10^7 N/m^2$ and E_{net}=$5 \times 10^{10} N/m^2$, which correspond to a realistic full-scale value and to an almost rigid net. Numerical results show that the net elasticity has a small effect on the anchor force as long as it is in a reasonable region. The point weight that attached to the bottom of the net is also varied and very small deviation is observed.

Mooring system: The pretension forces in the front two anchor lines are asymmetric with respect to x-axis in the model tests, as is explained in section 2. Asymmetric pretension forces are used in nominal simulations

and negligible difference is observed if mean pretension forces are adopted. The anchor load does not seem to be sensitive to the stiffness of the springs in the anchor lines, the weight of the anchor chain and the drag forces on the buoys.

4.2. Combined waves and current

In this section, we present the numerical results of the mooring loads in the front two anchor lines and front two bridle lines when the system is exposed to combined waves and current. Experimental data are used to validate the numerical results. Similar with that in current cases, nominal numerical results are shown at first, then a detailed sensitivity analysis is conducted, identifying the dominant parameters influencing the mooring loads.

4.2.1. Nominal results

A convergence study is performed and the mesh $N_H \times N_V = 20 \times (8{+}6)$ is found to be sufficient to reach convergence and is used in nominal simulations. Snapshots showing the floating collar, net cage, sinker tube and mooring lines are given in Figure 9 for cases in wave only and in combined wave and current. The linear incident wave profile is included. Since the considered wave is relatively long (wave length-to-floating collar diameter ratio λ/D=1.12), the floating tubes basically follow the wave. Taking a close look at the upper right two snapshots, we can see that the front two bridle lines get slack. This means that the bridle lines may experience snap loads. The latter consequence is not included in the analysis, but needs to be considered in future work in a similar way as done by Bardestani and Faltinsen (2013).

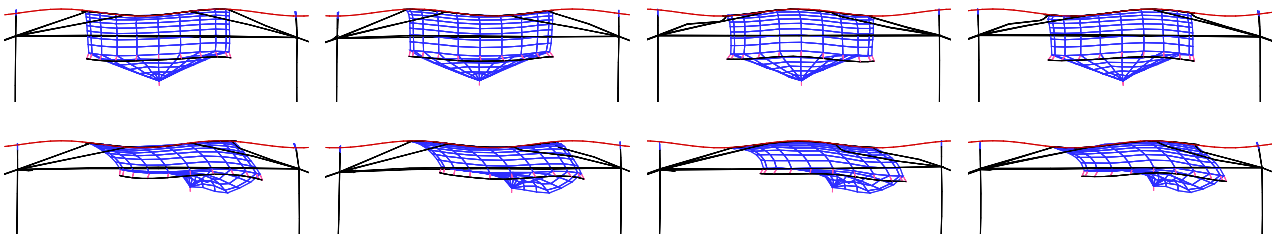

Figure 9: Upper row: snapshots for different time-steps from numerical simulations with $N_H \times N_V = 24 \times (8+6)$ (wave only). Wave period T=6s and wave height H = 2.5m. Lower row: snapshots for different time-steps from numerical simulations (combined wave and current). Current velocity U_∞ = 0.5m/s, wave period T=6s and wave height H = 2.5m.

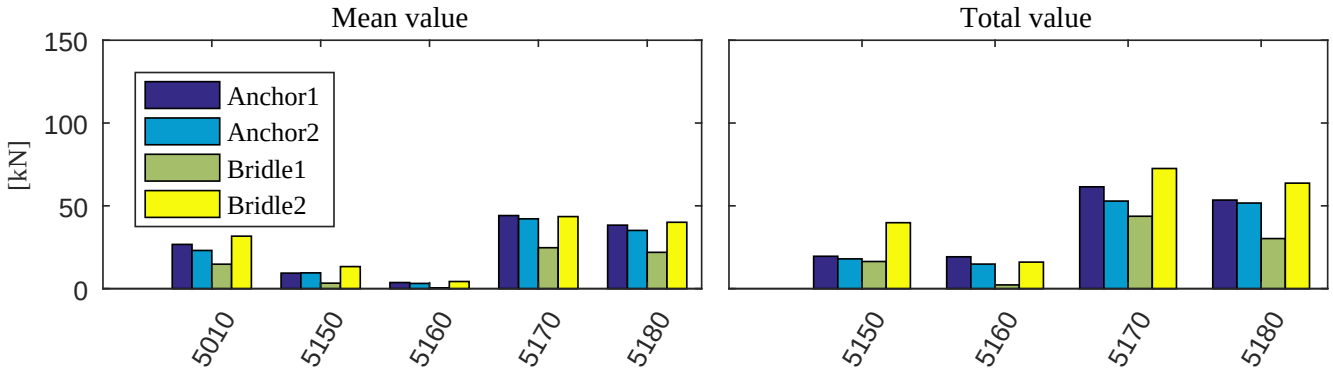

Figure 10: Mean and peak (total) values of the mooring loads in the front two anchor lines and bridle lines, obtained from experiments. The pretension force is subtracted. The positions of the anchor lines and bridle lines are illustrated in Figure 1. Detailed test information of different test numbers is shown in Table 4. Test 5010: current only. Test 5150 and 5160: waves only. Test 5170 and 5180: combined waves and current.

Before going to detailed analysis, we first show the mooring loads in the anchor lines and bridle lines from the model tests, see Figure 10. From the figure, we can have the following conclusions: the loads in the two anchor lines are similar if the pretension forces are subtracted; load in the bridle line-2 is about twice that in the bridle line-1; the forces in the anchor lines and in the bridle line-2 are similar. In the following analysis, we will focus on

the average value of the loads in the front two anchor loads (anchor load) and the load in the bridle line-2 (bridle load).

Nominal results for the anchor load and bridle load are presented in Figure 11 and 12 and are compared with the experimental data. Just the peak (total) values are investigated. Two wave steepness ($H/\lambda = 1/40$ and $1/22$) and two current velocities (U_∞=0.0m/s and 0.5m/s) are considered. In general, the agreement is fair for both the anchor load and the bridle load. Two different sinker tube weights with W_s=25kg/m and 50kg/m are investigated and numerical results indicate that the sinker tube weight has a small influence on the mooring loads for wave only cases. For combined waves and current cases, system with larger sinker tube weight experiences larger mooring loads due to smaller deformations of the net cage.

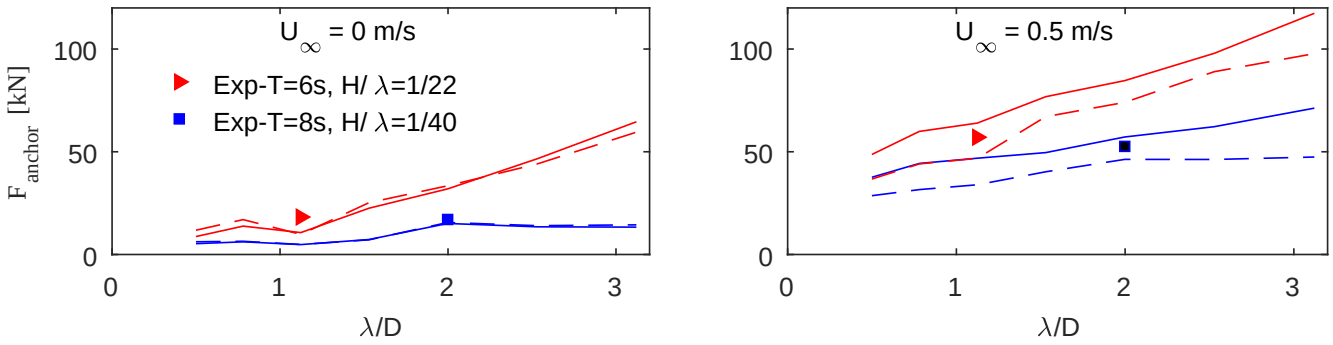

Figure 11: Comparison of the anchor loads (total) from the model tests (solid symbols) and present numerical simulations (solid curves) with sinker tube weight W_s = 50 kg/m. Pretension force is subtracted. Results are presented versus wave length-to-diameter ratio λ/D. Here D is the mean value of the center line diameter of the two tubes of the floating collar. Two wave steepness are considered with H/λ = 1/22 and 1/40. Numerical results with sinker tube weight W_s=25 kg/m are also shown (dashed line). Left: wave only. Right: combined waves and current with current velocity U_∞ = 0.5 m/s.

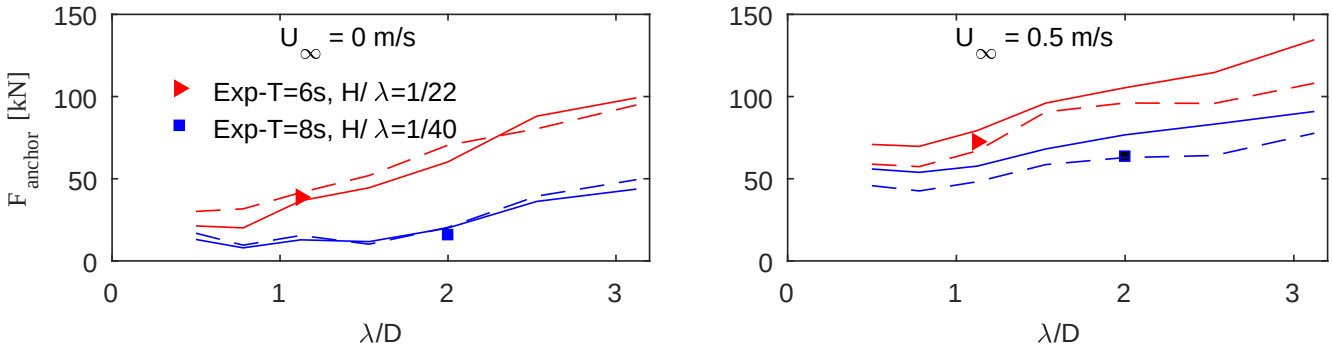

Figure 12: Same as in Figure 11, but for the bridle line-2.

4.2.2. Numerical sensitivity analysis

A sensitivity analysis is performed for the system in regular waves only and in combined regular waves and current. The focus is on the peak (total) values of the mooring loads. The parameters examined are shown in Table 5. The majority of the parameters are the same as cases in current only, but with some additional wave related parameters. The condensed results for the anchor load are presented in Figure 13 and 14. In Figure 13, each bar represents the percentage difference of the anchor load with respect to the nominal value, averaged over all the wave periods. In Figure 14 each bar represents the mean of the absolute value of the condensed data presented in Figure 13. Parameters that impose more than 5% difference with respect to nominal value for wave only cases and combined waves and current cases, are marked by "×" in the last two columns in Table 5. From Figure 13, we can see that modeling the sinker tube as a rigid body has a most pronounced effect on the anchor load for cases in waves only. This is maybe due to that a rigid sinker tube will change the deformation of the net in vertical direction, as a rigid sinker tube cannot deform accordingly with the floating collar which follows the wave profile. In combined

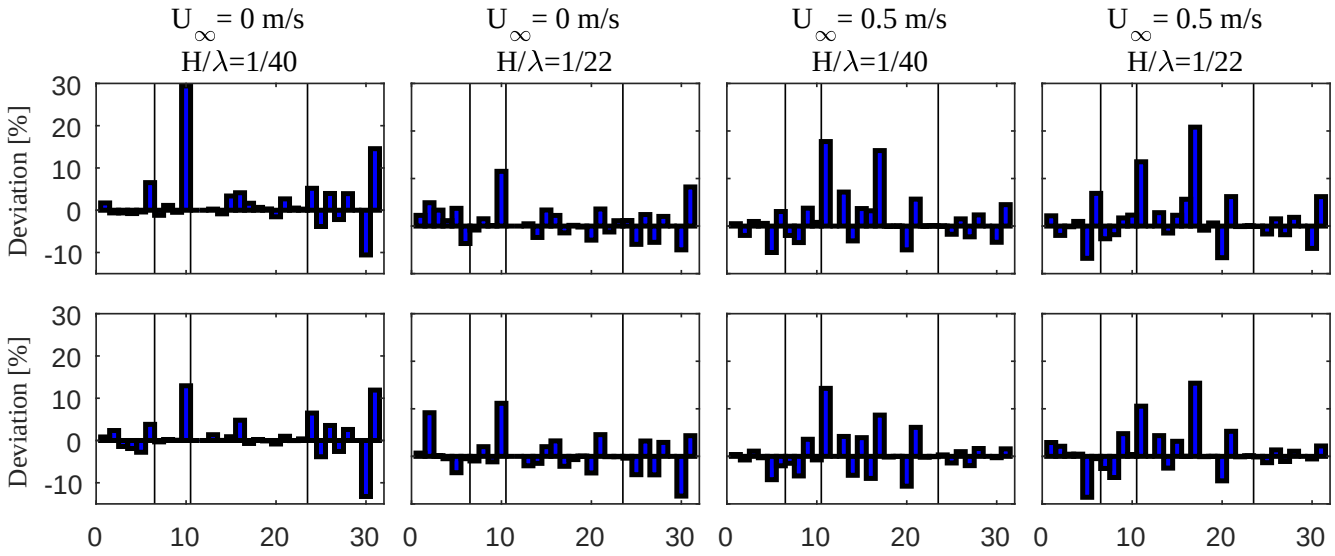

Figure 13: Each bar represents the percentage difference of the anchor load with respect to the nominal value, averaged over all the examined wave periods. The numbers on the horizontal axis refer to variation number as given in Table 5. Upper row: sinker tube with weight 25 kg/m. Lower row: sinker tube with weight 50 kg/m.

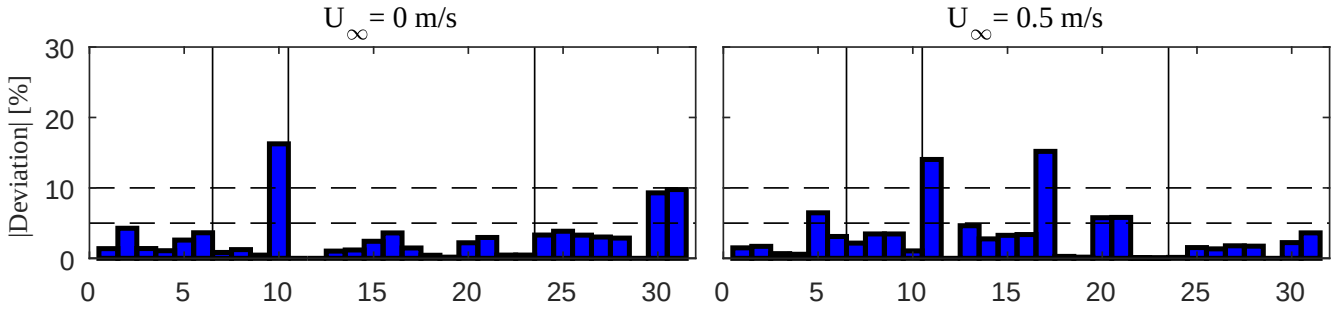

Figure 14: The mean of the absolute value of the condensed data presented in Figure 13.

waves and current cases, the flow reduction factor r in the rear part of the net and the diameter of the net cage (conical part) are the two important parameters. In terms of the modeling of the floating collar, simplifications can be made with limited errors, such as modeling the floating collar as a rigid body, neglecting the axial stiffness due to axial tensions and using zero frequency instead of the three-dimensional frequency-dependent added mass. Also numerical results indicate that considering nonlinear Froude Kriloff and restoring forces for the floating collar is not necessary. In general, the loads on the floating collar are quite moderate compared with forces on the whole system.

Sensitivity analysis for the bridle load is also conducted and results are shown in Figure 15 and 16. Figure 16 clearly shows that modeling the floating collar as a rigid body has a pronounced effect on the bridle load, this is because rigid floating collar significantly changes the force distribution along the bridle lines.

4.3. Irregular sea

In this section, the fish farm system in irregular waves is investigated. In Figure 17, we present the mean and maximum values of the mooring loads in the front two anchor lines and front two bridle lines from experiments. The duration of the irregular waves in the model tests is 1.5 hour. The pretension forces are subtracted. From the figure, we can have the following conclusions: the mean values of the mooring loads for cases with different significant wave heights and peak wave periods are similar while there is a big difference in the maximum values; the tension in the bridle line-2 is about twice than that in the bridle line-1; the mean values of the tensions in the bridle line-2 and in the anchor lines are similar, but the maximum tension in the bridle line-2 is much larger. We

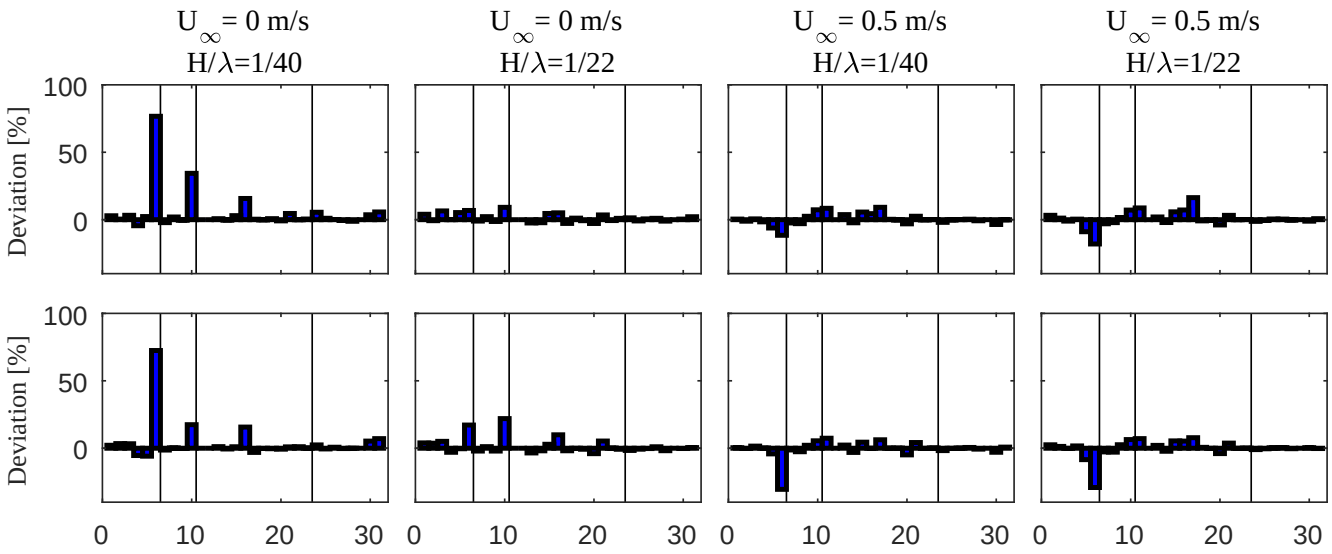

Figure 15: Same as in Figure 13, but for the bridle load.

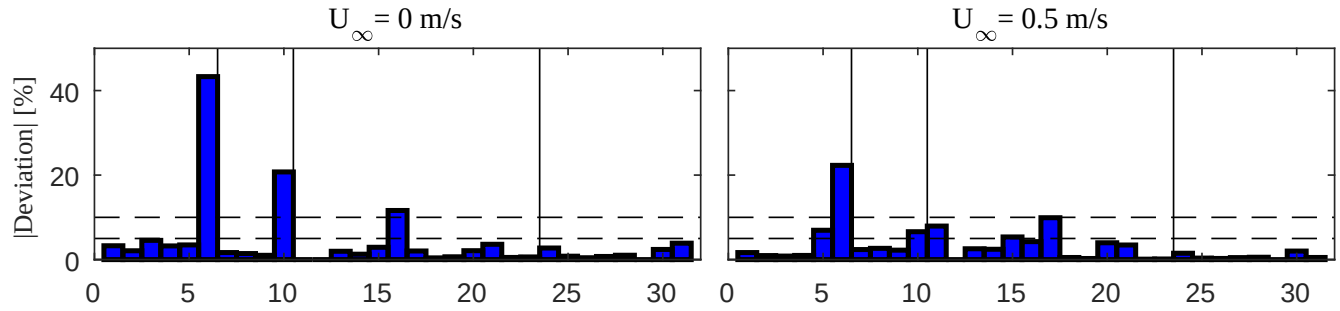

Figure 16: The mean of the absolute value of the condensed data presented in Figure 15.

will focus on the average value of the loads in the front two anchor lines (anchor load) and the load in the bridle line-2 (bridle load) in the following analysis.

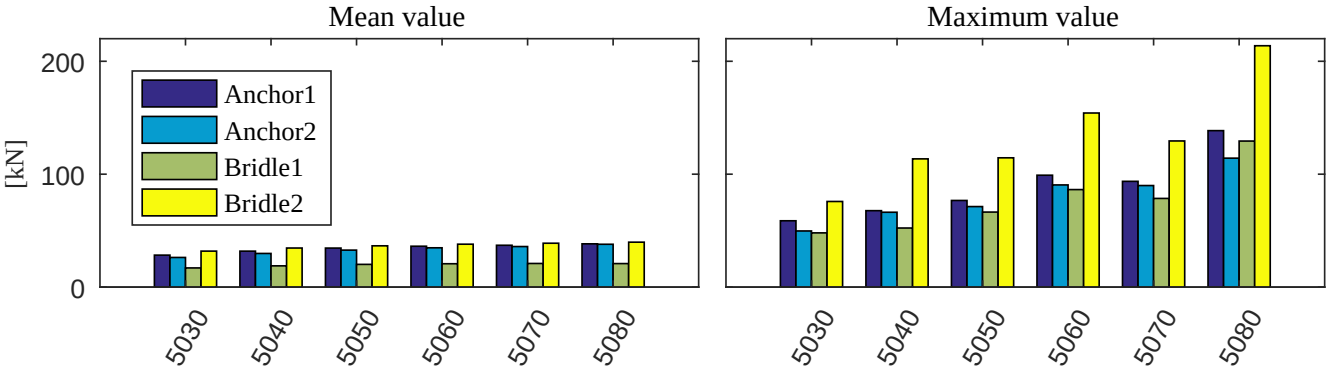

Figure 17: Mean and maximum values of the tensions in the front two anchor lines and front two bridle lines, obtained from experiments for the system in irregular waves. The pre-tension force is subtracted. The positions of the anchor lines and bridle lines are illustrated in Figure 1. Detailed test information of different test numbers is shown in Table 4. From left to right: with increasing significant wave height and peak wave period.

Figure 18 shows the comparison of the mean, standard deviation and maximum values of the anchor loads from numerical simulations and the experiments. The same wave duration is considered in the simulations as

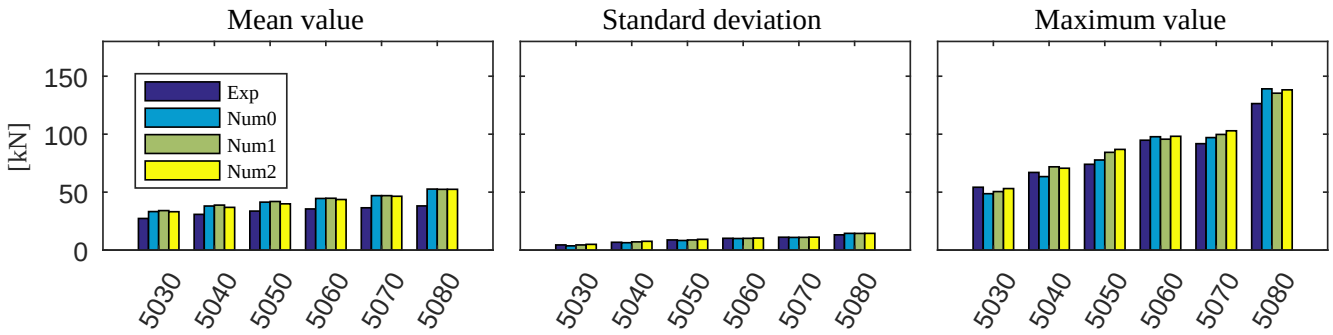

Figure 18: Comparison of mean, standard deviation and maximum values of the anchor loads from the model tests and present numerical simulations for the fish farm system in irregular waves. Detailed test information of different test numbers is shown in Table 4. Num0, Num1 and Num2 denote nominal results, results using zero frequency added mass for different modes of the floating collar and results considering a rigid floating collar, respectively.

that in the model tests. From the figure, we can see that general agreement between the numerical (nominal) and experimental results of the mean, standard deviation and maximum values of the anchor loads is fair and numerical results slightly over-predict the mean values which is similar with that in current only cases. It should be noted that the random phase seeds used in the experiments to generate the incident irregular waves are different with respect to those used in the simulations. The ratio of the maximum anchor load (minus mean value) to the standard deviation varies from 4.6 to 6.7 according to the experimental data. The drag load on the net cage has the dominant contribution to the total load, which is similar with the case when Morison's equation is used to estimate the wave load. So we can have a rough estimation of the probability distribution of the maximum anchor load based on the statistics characteristics of the Morison-type forces for random seas. It is assumed that the wave elevation process is a stationary Gaussian process. Then according to Naess and Moan (2012), in the absence of current, the distribution of the maximum value for Morison-type force depends on the relative importance of the drag and inertial forces. If the inertial force is dominant, then Rayleigh distribution can be used to describe the distribution of the maximum value. Then the most probably maximum value (minus mean value) can be approximately estimated by 4 $\times$ standard deviation for a short time description of wave elevation in the range from 1/2 hour to 10 hour. Actual ratio depends on the the duration of the sea state and the mean wave period. If the drag force is dominant, then exponential distribution can be adopted and higher most probable largest values are expected. For the fish farm system, the distribution of the maximum value of the anchor load should be a combination of Rayleigh distribution and exponential distribution and the most probable largest value should be larger than 4 $\times$ standard deviation, which means that the experimental results are reasonable.

In the nominal simulations, the hydrodynamic radiation loads for different modes (both elastic and rigid) of the floating collar are expressed in terms of convolution integrals with retardation functions according to linear potential-flow theory. Numerical results using zero frequency added mass for different modes and modeling the floating collar as a rigid body are also shown in Figure 18. The numerical results indicate that the effect of the elasticity of the floating collar on the anchor load is rather moderate and simplified hydrodynamic model for the floating collar is enough to reach desired accuracy.

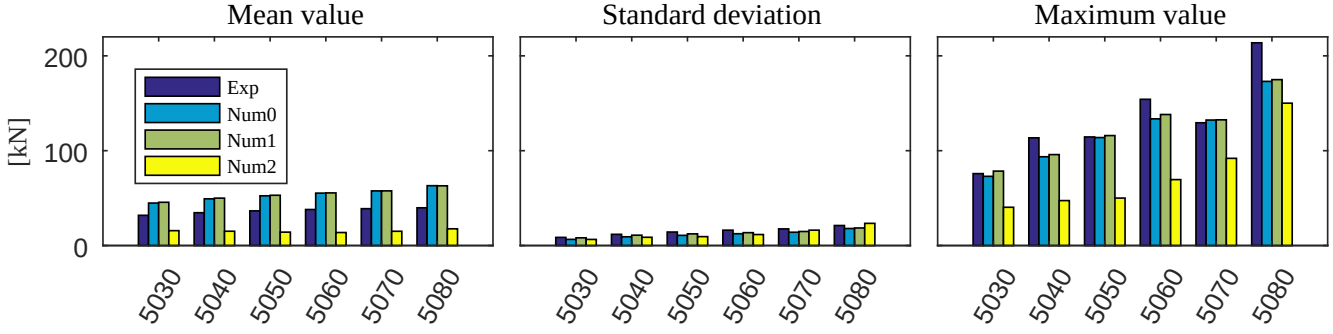

Figure 19: Same as in Figure 18, but for the bridle line-2.

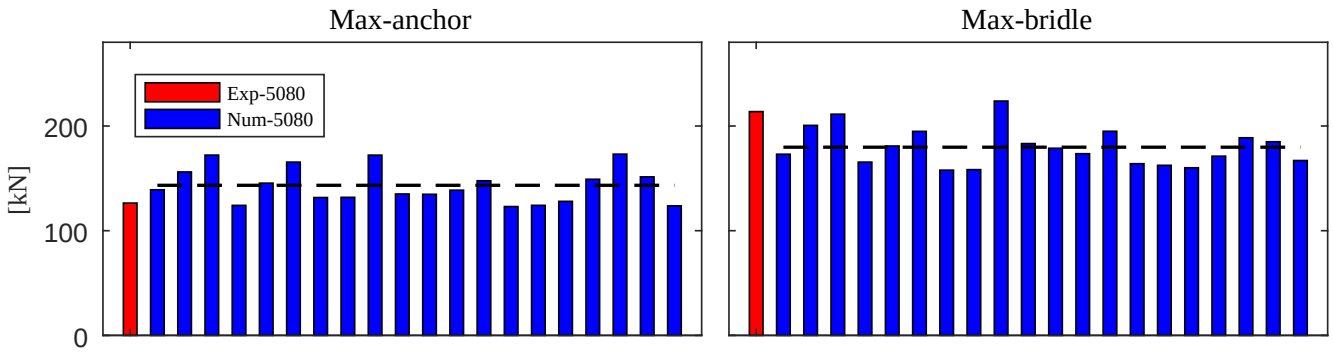

Figure 20: Comparison of the mooring loads (maximum value) obtained from the experiment and numerical simulations for case 5080. The first bar represents the experimental data, the rest are numerical results but with different random phase seeds to generate the incident irregular waves. Dashed line represents the most probable maximum value obtained as mean among the maximum values from numerical simulations. Left: anchor load. Right: bridle load.

In Figure 19, we present the loads in the bridle line-2 from the numerical simulations and the experiments. Both the nominal numerical results and results using zero frequency added mass for different modes and modeling the floating collar as a rigid body are shown in the Figure. The figure shows that modeling the floating collar as a rigid body has a significant influence on the bridle load, as it will change the force distribution between bridles. Numerical simulations with different random phase seeds (in total 20) to generate the incident irregular waves are performed and the comparison of the maximum values of the mooring loads between the numerical and experimental results for case 5080 is shown in Figure 20. The figure shows that there is a big variation of the maximum loads in the anchor line and in the bridle line when different random phase seeds are used in the numerical simulations. The maximum anchor loads from numerical predictions vary from 98% to 136% of that from the experiment and the maximum bridle loads change from 74% to 105% of the experimental data. As an engineering practice, at least 10-20 realizations of the same wave spectrum are needed to have a robust estimation of the most probable maximum value which is taken as the mean value of these realizations. In order to have a better comparison of the most probable maximum value between numerical and experimental results, more realizations of the same spectrum in the experiments are needed.

4.4. Survival conditions

The aquaculture industry is trying to move the fish farms from nearshore to more exposed sea regions. However, a question remains to be answered: is it feasible to use the conventional fish farm concept to operate in exposed area and how exposed it can operate. In this section, the proposed numerical method is used to examine the responses of a conventional floating collar fish farm system in different exposure scenarios and in this respect to determine the survival conditions of the system. First, we should choose proper criteria to determine the survival conditions. From the structural perspective, the major components should be strong enough to withstand the environmental loads in exposed regions. For the mooring system, the maximum load in the mooring line should not yield its breaking limit. In terms of the floating collar, it basically follows the waves and may experience large deformations in severe sea states, so we should guarantee that it will not collapse. Since the sinker tube is attached directly to the net in the present study, we can avoid the possible chafing between the vertical chains and the net (dominant cause for fish escape). Also, the force acting on the sinker tube is quite moderate, so both the net cage and the sinker tube should not be of a major concern. In addition, enough net cage volume is required for the welfare of the fish. In summary, from the perspective of fish welfare and structural integrity, three criteria are proposed to determine the survival conditions, i.e. maximum forces in the mooring lines; maximum stress in the floating collar and maximum reduction of net cage volume.

The simulation matrix is shown in Table 6. The different fish farm set-ups considered are also shown in the table. Detailed information of the wave conditions and the corresponding wave classes according to the Norwegian Standard are given in Table 7.

4.4.1. Current only

First, we present results for cases in current only. The current velocity is chosen from small exposure to high exposure. The anchor loads and the net cage volume reductions in different current velocities are shown in Figure

Table 6: Environmental matrix used in simulations, showing current velocity, wave steepness and wave period ranges. The different combinations of the sinker tube weight (or discrete sinker weights) and point weight (attached to the bottom of the net cage) are also shown in the lower table. If discrete sinker weights instead of the sinker tube are adopted, the discrete sinker weights are chosen to have the same total submerged weight as that of the sinker tube.

Current U_∞ [m/s]	Wave steepness H/λ		
	1/60	1/30	1/15
0.0	4-10s	4-10s	4-10s
0.3	4-10s	4-10s	4-10s
0.5	4-10s	4-10s	4-10s
0.7	4-10s	4-10s	4-10s
0.1-1.2	-	-	-

Sinker tube weight (w_s)	25 kg/m	50 kg/m	80 kg/m	93 kg/m
Discrete sinker weights (W_s)	203 kg	407 kg	651 kg	757 kg
Center point weight (W_c)	200 kg	500 kg	1000 kg	1500 kg

Table 7: Detailed information of the wave conditions described in Table 6. The corresponding wave class according to the Norwegian Standard (see Table 1) for regular waves is given in the right table.

T [s]	λ [m]	λ/D [m]	$H/\lambda = 1/60$	1/30	1/15
			H[m]		
4	25.0	0.50	0.42	0.83	1.66
5	39.0	0.78	0.65	1.30	2.60
6	56.2	1.12	0.94	1.87	3.75
7	76.5	1.53	1.27	2.55	5.10
8	99.9	2.00	1.66	3.33	6.66
9	126.4	2.53	2.10	4.21	8.43
10	156.0	3.12	2.60	5.20	10.40

Wave	Exposure	$H = 1.9H_s$
A	Small	H <1.0 m
B	Moderate	1.0 m< H <1.9 m
C	Heavy	1.9 m< H <3.8 m
D	High	3.8 m< H <5.7 m
E	Extreme	5.7 m< H

21. The net cage volume is estimated by

$$V = -\iint_{S_c} n_1 x dS = -\iint_{S_c} n_2 y dS = -\iint_{S_c} n_3 z dS \tag{13}$$

where V is the net cage volume, $\mathbf{n} = (n_1, n_2, n_3)$ the normal vector of the cage surface S_c and is pointing outwards. The net volume is taken as the average value of the volumes estimated numerically with the three formulas in Eq. (13). From the figure we can see that the difference is small in the anchor loads when we use the sinker tube or the discrete sinker weights to keep the net cage volume. However, relatively big difference in the net cage volume reduction is observed between the two options, especially for medium current velocities. The numerical results demonstrate that the sinker tube is more suitable to be used to keep the net cage volume. The maximum cage volume reduction is set to be 60% as a operational limit for the sake of fish welfare. The figure shows that the fish farm with sinker tube weight w_s=93 kg/m and center point weight W_c=1500 kg can operate in current velocity up to 0.85 m/s which is in the region of high exposure.

4.4.2. Combined waves and current

Then, numerical results for the anchor forces for cases in combined waves and current are given in Figure 22. Just the peak (total) values are shown. Four current velocities and three wave steepnesses are considered, covering the range of wave class from small exposure to extreme exposure. The figure shows that the difference of the anchor force is small when the sinker tube and the discrete sinker weights are used, respectively, similarly as in the cases in current only. The minimum breaking force for the considered anchor polysteel ropes is about 430 kN, which is

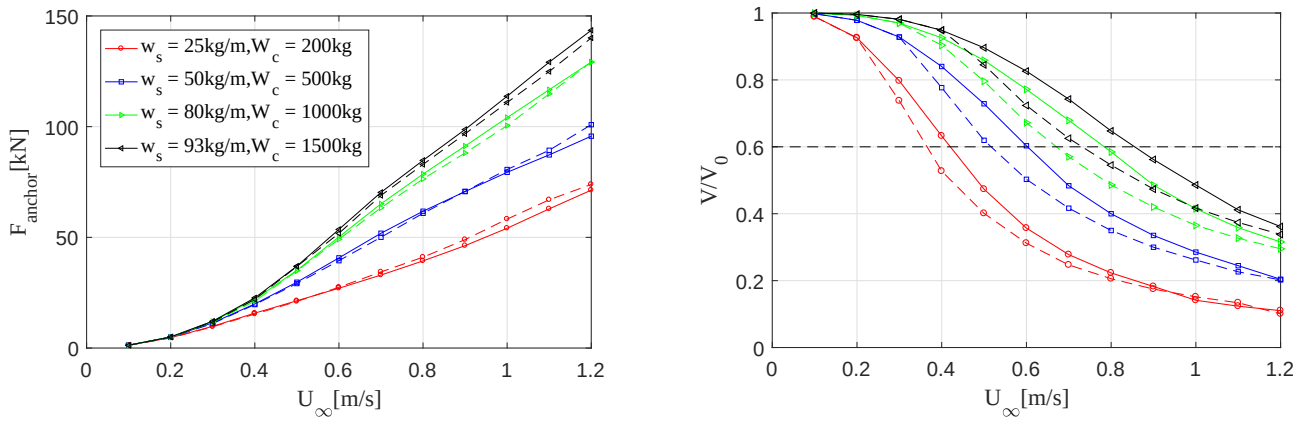

Figure 21: Numerical predictions of the mean load in the front two anchor lines (left) and the net volume reductions (right) for cases in current only with different fish farm set-ups, see Table 6. Solid line: sinker tube (w_s). Dashed line: discrete sinker weights (W_s). Right: V_0 is the initial volume of the net cage, V the net volume in steady-state.

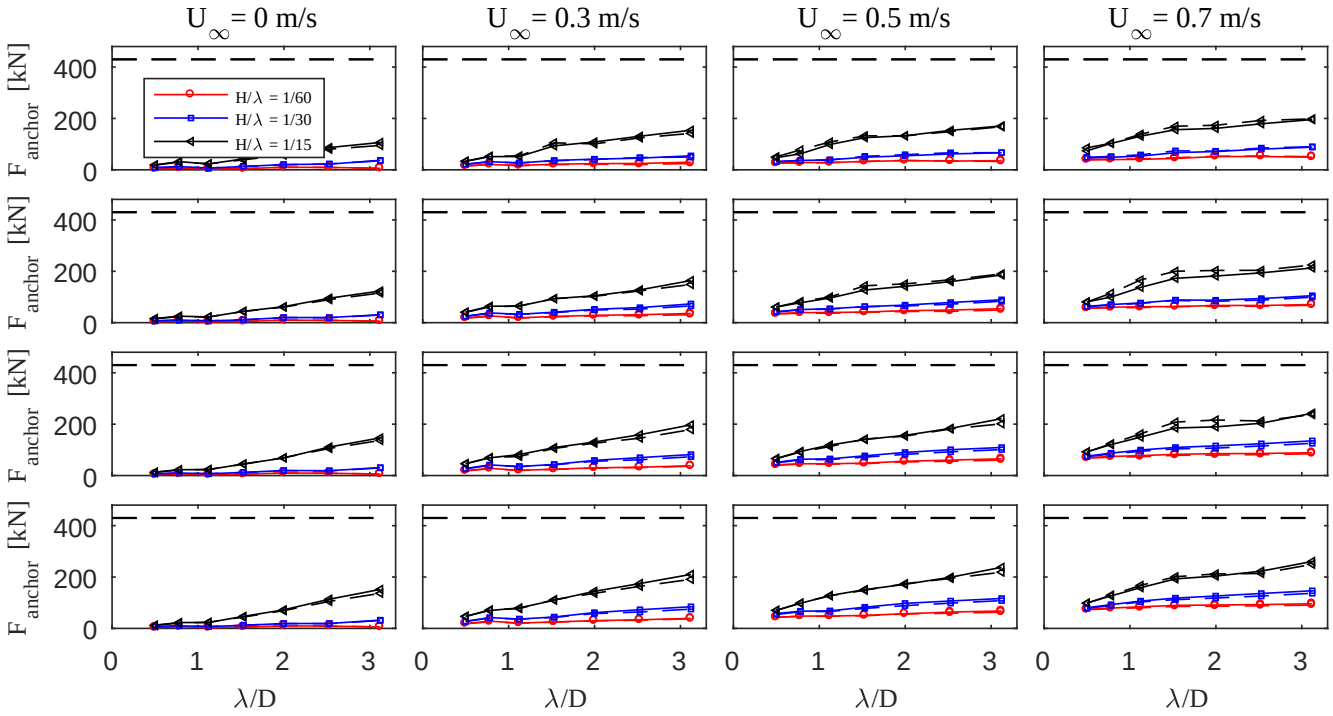

Figure 22: Mean load in the front two anchor lines for cases in combined regular waves and current with different fish farm set-ups. Results are presented versus wave length-to-diameter ratio λ/D. Solid line with symbols: sinker tube. Dashed line with symbols: discrete sinker weights. From left to right: current velocities U_∞ = 0 m/s, 0.3 m/s, 0.5 m/s, 0.7 m/s. From top to bottom: sinker tube weights w_s = 25 kg/m, 50 kg/m, 80 kg/m and 93 kg/m. Dashed line represents the minimum breaking force (polysteel, 3 strand, diameter 52 mm).

larger than the maximum force experienced by the anchor lines, so the anchor loads are not the main concern for the fish farm system to operate in exposed regions.

Figure 23 shows the numerical predictions of the loads in the bridle line-2. In general, the load in the bridle line-2 is slightly larger than that in the anchor lines. However the bridle lines are weaker than the anchor lines in reality, which should be paid special attention during the design. The maximum force in the bridle line may exceed its breaking limit in high to extreme exposure sea states. It should be noted that the loads in the bridle lines are strongly dependent on the arrangement of the bridle lines, so the load distribution between bridle lines may be totally different from the present set-up if a new mooring system is considered.

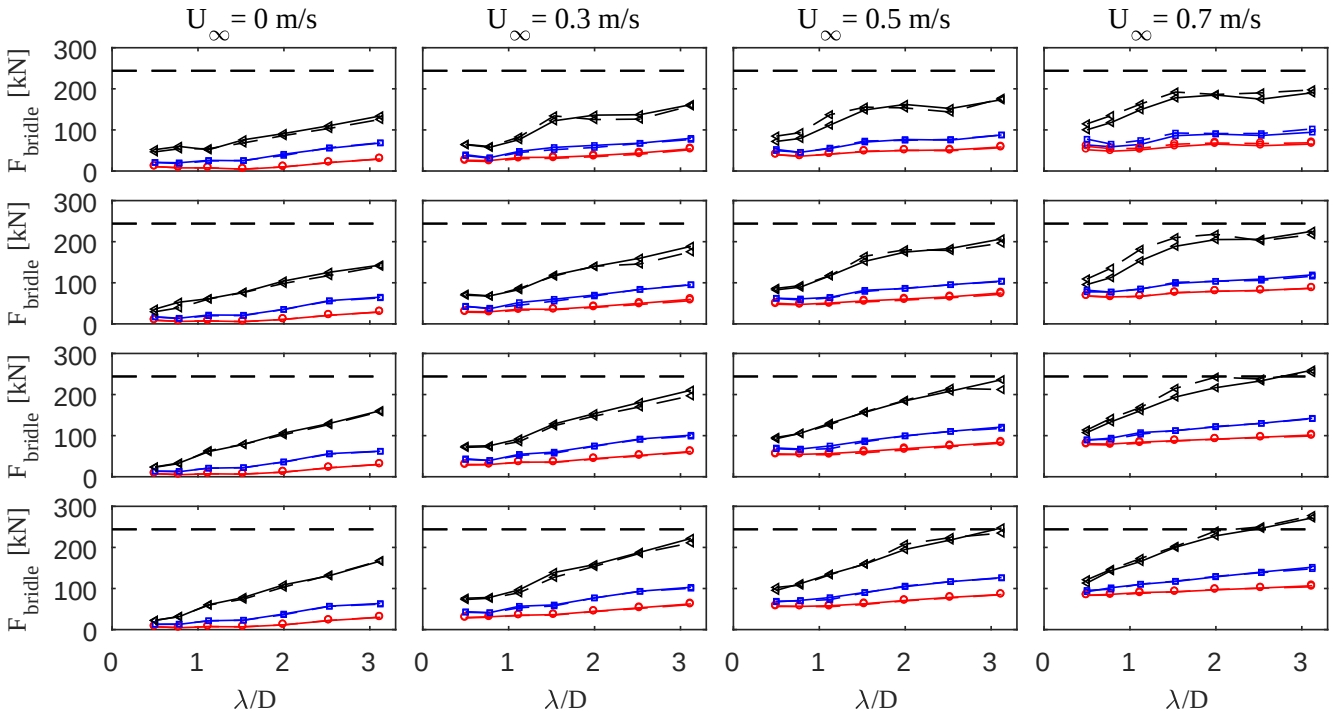

Figure 23: Same as that in Figure 22, but for the bridle line-2. Dashed line represents the minimum breaking force (polysteel, 3 strand, diameter 40 mm).

In order to see how irregular waves are represented by regular waves according to the standard in Table 1, we present the maximum values of the anchor loads and the bridle loads in Figure 24 for the system in both irregular and equivalent regular waves. The figure shows that the maximum mooring loads are similar for the considered two wave types and results from regular waves are generally more conservative, which coincides with the conclusion from Berstad and Tronstad (2005). It should be noted that just one realization is considered for the irregular sea scenario and actual results in irregular sea are realization dependent.

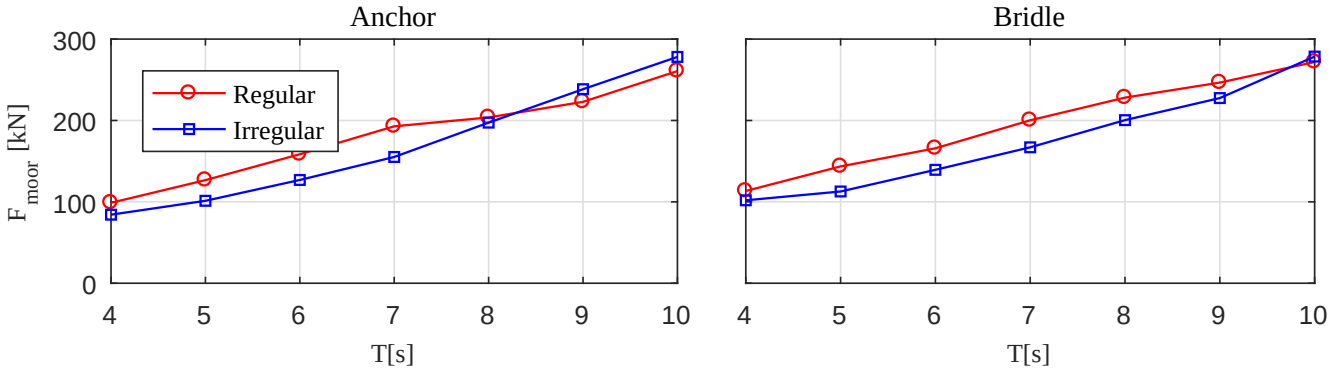

Figure 24: Comparison of the maximum loads in the anchor line (left) and bridle line (right) by numerical calculations in irregular waves and equivalent regular waves. The considered regular wave steepness $H/\lambda = 1/15$, current velocity $U_\infty = 0.7$ m/s.

The results of the net volume reductions for the system in combined waves and current are also investigated and are not shown here. The general conclusion is that the cage volume reduction is dominated by the current in mild wave conditions, however in cases with high wave steepness, both the current and wave will have equivalent contributions.

Finally, we show the numerical predictions of the stress distributions along the floating collar. The maximum

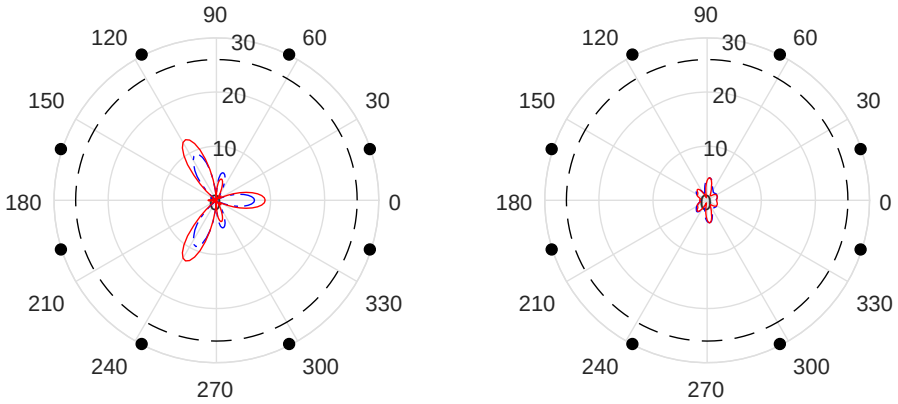

Figure 25: Stress distributions along the floating collar for cases with U_∞=0.7 m/s, H/λ =1/15 and T=8 s (dashed dot line) and T=10 s (solid line). Left: stress due to horizontal deformations. Right: stress due to vertical deformations. Dashed line represents the yield stress (high-density polyethylene). Solid circle symbols represent the positions where bridle lines are attached.

bending stress due to horizontal deformations in a position $x = R\cos\beta$ along the floater is given as

$$\sigma(\beta, t) = \frac{M(\beta, t)}{I} r_{\max} = \frac{E r_{\max}}{R^2} \sum_{n=2}^{\infty} n^2 b_n(t) \cos n\beta \tag{14}$$

where E is the Young's modulus, I is the area moment of the cross section in horizontal plane and $r_{\max} = 3c_f$ with c_f the cross-sectional radius of the floating collar which comprises two tubes and are placed with center to center distance $4c_f$. Similar expression can be obtained for the stress due to vertical deformations. One should mention that the area moment of the cross section in horizontal plane is about 10 times that in vertical plane. The stress distributions along the floating collar due to horizontal and vertical deformations are shown in Figure 25. The figure shows that the stress due to vertical deformations are small compared with that from horizontal deformations and the maximum stress occurs at the positions $\beta = 117^0$ and 243^0 where bridle lines are attached. The maximum stress along the floating collar will not exceed the yield stress of the floating collar for the considered sea states.

5. Conclusions

We presented a study on a realistic fish farm system with single cage exposed to current, regular and irregular waves. The system comprises a floating collar with two concentric tubes, a flexible net cage and a sinker tube attached directly to the net, moored by a complex mooring system with anchor lines, bridle lines and frame lines. A numerical solver was developed and implemented. The curved beam equations with consideration of hydroelasticity were adopted for solving the motions of the floating collar and the sinker tube. The net cage was modeled by a truss model and the hydrodynamic forces on the cage were predicted by a screen model which accounts for hydrodynamic shadow and Reynolds number effect. Loads in the anchor lines and in the bridle lines were investigated in detail and satisfactory agreement between numerical and experimental results was demonstrated for the system in both regular and irregular waves. One thing interesting was that the load in one of the bridle lines was larger than the rest of the mooring loads for most of the cases, nevertheless the bridle lines in reality are weaker than the remaining mooring lines.

A systematic sensitivity analysis was performed to identify the dominant factors when modeling the fish farm in regular waves and current. The main focus is on the mooring loads. In total 31 parameters from different components were analyzed separately. The study suggested that the mooring loads in the anchor lines and in the bridle lines were not sensitive to the majority of the variations. The most important parameter for the anchor loads is the flow reduction factor in the rear part of the net cage. Modeling the floating collar as a rigid body has a moderate effect on the anchor loads, but the bridle loads may differ by more than 20% as it will change the force distribution along bridles. The mooring loads are not sensitive to the wave load model for the floating collar and hydrodynamic forces on the floating collar are quite moderate compared with the total loads on the system for cases in both regular and irregular waves.

Finally, fish farms with different set-ups in different exposure scenarios were investigated numerically. The considered wave periods, wave steepness and current velocities cover the sea states from light exposure to extreme exposure, according to the Norwegian standard for regular waves. The main target was to figure out the main constraint for the conventional fish farms to operate in exposed areas and how exposed they can operate. Three criteria were proposed: maximum net cage volume reduction, maximum loads in the mooring lines and maximum stress in the floating collar. Numerical results showed that the net volume reduction was the dominant limit. The maximum stress in the floating collar was moderate compared with the yield stress of the floating collar, even for extreme sea states. In terms of the mooring system, the existing mooring system can be applied in offshore area if the bridle lines are properly designed.

In the paper, the studies in survival conditions just examined the most critical scenario with aligned long crested waves and current. It means that the conclusions may be a bit conservative. The fish farm system in more general sea states should also be studied and possibly three-dimensional waves should be accounted for; this is left for a future work. Their implementation in the present method is relatively straightforward within the assumption of linear superposition principle. The influence of the arrangement of the bridle lines on the mooring loads should also be considered. The numerical solver proposed in this paper is applicable to any net-based fish farm concepts and can be used to analyze fish farms, for instance, with submersible net cages or square net cages. However, how to account for the effect of upstream cages on current in case with multiple cages needs to be further studied.

Acknowledgement

This work was supported by the Research Council of Norway through the Centers of Excellence funding scheme AMOS, project number 223254.

References

Bardestani, M., Faltinsen, O. M., 2013. A two-dimensional approximation of a floating fish farm in waves and current with the effect of snap loads. In: ASME 2013 32nd International Conference on Ocean, Offshore and Arctic Engineering. American Society of Mechanical Engineers, pp. V009T12A020–V009T12A020.

Berstad, A., Tronstad, H., 2005. Response from current and regular/irregular waves on a typical polyethylene fish farm. Proceedings from Maritime Transportation and Exploitation of Ocean and Coastal Resources (IMAM).

Bi, C.-W., Zhao, Y.-P., Dong, G.-H., Xu, T.-J., Gui, F.-K., 2014a. Numerical simulation of the interaction between flow and flexible nets. Journal of Fluids and Structures 45, 180–201.

Bi, C.-W., Zhao, Y.-P., Dong, G.-H., Zheng, Y.-N., Gui, F.-K., 2014b. A numerical analysis on the hydrodynamic characteristics of net cages using coupled fluid–structure interaction model. Aquacultural Engineering 59, 1–12.

Dong, G.-H., Xu, T.-J., Zhao, Y.-P., Li, Y.-C., Gui, F.-K., 2010. Numerical simulation of hydrodynamic behavior of gravity cage in irregular waves. Aquacultural Engineering 42 (2), 90 – 101.

Faltinsen, O., 1990. Sea loads on ships and ocean structures. Cambridge University, Cambridge, UK.

He, Z., Faltinsen, O. M., Fredheim, A., Kristiansen, T., 2015. The influence of fish on the mooring loads of a floating fish farm. In: Proceedings 7th International Conference on Hydroelasticity in Marine Technology.

Huang, C.-C., Tang, H.-J., Liu, J.-Y., 2006. Dynamical analysis of net cage structures for marine aquaculture: Numerical simulation and model testing. Aquacultural Engineering 35 (3), 258–270.

Kristiansen, D., 2010. Wave induced effects on floaters of aquaculture plants. Ph.D. thesis, Norwegian University of Science and Technology, Trondheim, Norway.

Kristiansen, T., Faltinsen, O. M., 2012. Modelling of current loads on aquaculture net cages. Journal of Fluids and Structures 34, 218–235.

Kristiansen, T., Faltinsen, O. M., 2015. Experimental and numerical study of an aquaculture net cage with floater in waves and current. Journal of Fluids and Structures 54, 1–26.

Lader, P. F., Fredheim, A., 2006. Dynamic properties of a flexible net sheet in waves and current: A numerical approach. Aquacultural engineering 35 (3), 228–238.

Lee, C.-W., Kim, Y.-B., Lee, G.-H., Choe, M.-Y., Lee, M.-K., Koo, K.-Y., 2008. Dynamic simulation of a fish cage system subjected to currents and waves. Ocean Engineering 35 (14), 1521 – 1532.

Li, P., Faltinsen, O. M., 2012. Wave-induced vertical response of an elastic circular collar of a floating fish farm. In: The 10th International Conference on Hydrodynamics (ICHD 2012). St. Petersburg, Russia.

Li, P., Faltinsen, O. M., Lugni, C., 2016. Nonlinear vertical accelerations of a floating torus in regular waves. Journal of Fluids and Structures 66, 589–608.

Løland, G., 1991. Current forces on and flow through fish farms. Division of Marine Hydrodynamics, the Norwegian Institute of Technology.

Marichal, D., 2003. Cod-end numerical study. In: Third International Conference on Hydroelasticity in Marine Technology.

Moe, H., Fredheim, A., Hopperstad, O., 2010. Structural analysis of aquaculture net cages in current. Journal of Fluids and Structures 26 (3), 503–516.

Naess, A., Moan, T., 2012. Stochastic dynamics of marine structures. Cambridge University Press.

Nygaard, I., 2013. Merdforsøk. kapasitets-tester. interaksjon mellom not og utspilingssystem. Tech. rep., Tech. rep., Norsk Marinteknisk Forskningsinstitutt AS.

StandardNorge, 2009. Marine fish farms - requirements for site survey risk, analysis, design, dimensioning, production,installation and operation. NS 9415.

Xu, T.-J., Dong, G.-H., Zhao, Y.-P., Li, Y.-C., Gui, F.-K., 2011. Analysis of hydrodynamic behaviors of gravity net cage in irregular waves. Ocean engineering 38 (13), 1545–1554.

Xu, T.-J., Dong, G.-H., Zhao, Y.-P., Li, Y.-C., Gui, F.-K., 2012. Numerical investigation of the hydrodynamic behaviors of multiple net cages in waves. Aquacultural Engineering 48, 6–18.

Xu, T.-J., Zhao, Y.-P., Dong, G.-H., Gui, F.-K., 2013a. Analysis of hydrodynamic behavior of a submersible net cage and mooring system in waves and current. Applied Ocean Research 42, 155 – 167.

Xu, T.-J., Zhao, Y.-P., Dong, G.-H., Li, Y.-C., Gui, F.-K., 2013b. Analysis of hydrodynamic behaviors of multiple net cages in combined wave-current flow. Journal of Fluids and Structures 39, 222–236.

Yao, Y., Chen, Y., Zhou, H., Yang, H., 2016. Numerical modeling of current loads on a net cage considering fluid–structure interaction. Journal of Fluids and Structures 62, 350–366.

Zdravkovich, M., 1985. Forces on pipe clusters. In: Proc. Conf. on Separated Flow Around Marine Structures, Norwegian Institute of Technology, Trondheim. pp. 201–226.

Zhao, Y.-P., Bi, C.-W., Chen, C.-P., Li, Y.-C., Dong, G.-H., 2015. Experimental study on flow velocity and mooring loads for multiple net cages in steady current. Aquacultural Engineering 67, 24 – 31.

Zhao, Y.-P., Bi, C.-W., Dong, G.-H., Gui, F.-K., Cui, Y., Xu, T.-J., 2013. Numerical simulation of the flow field inside and around gravity cages. Aquacultural engineering 52, 1–13.

Zhao, Y.-P., Li, Y.-C., Dong, G.-H., Gui, F.-K., Teng, B., 2007. A numerical study on dynamic properties of the gravity cage in combined wave-current flow. Ocean engineering 34 (17), 2350–2363.

Zhao, Y.-P., Li, Y.-C., Dong, G.-H., Gui, F.-K., Wu, H., 2008. An experimental and numerical study of hydrodynamic characteristics of submerged flexible plane nets in waves. Aquacultural engineering 38 (1), 16–25.